



Spatial Distribution and Functional Impact of Human Scalp Hair Follicle Microbiota

Marta B. Lousada^{1,2}, Janin Edelkamp¹, Tim Lachnit², Markus Fehrholz¹, Irena Pastar³, Francisco Jimenez^{4,5}, Hanieh Erdmann⁶, Thomas C.G. Bosch² and Ralf Paus^{1,3,7}

Human hair follicles (HFs) constitute a unique microbiota habitat that differs substantially from the skin surface. Traditional HF sampling methods fail to eliminate skin microbiota contaminants or assess the HF microbiota incompletely, and microbiota functions in human HF physiology remain ill explored. Therefore, we used laser-capture microdissection, metagenomic shotgun sequencing, and FISH to characterize the human scalp HF microbiota in defined anatomical compartments. This revealed significant compartment-, tissue lineage-, and donor age-dependent variations in microbiota composition. Greatest abundance variations between HF compartments were observed for viruses, archaea, *Staphylococcus epidermidis*, *Cutibacterium acnes*, and *Malassezia restricta*, with the latter 2 being the most abundant viable HF colonizers (as tested by propidium monoazide assay) and, surprisingly, most abundant in the HF mesenchyme. Transfection of organ-cultured human scalp HFs with *S. epidermidis*-specific lytic bacteriophages *ex vivo* downregulated transcription of genes known to regulate HF growth and development, metabolism, and melanogenesis, suggesting that selected microbial products may modulate HF functions. Indeed, HF treatment with butyrate, a metabolite of *S. epidermidis* and other HF microbiota, delayed catagen and promoted autophagy, mitochondrial activity, and gp100 and dermcidin expression *ex vivo*. Thus, human HF microbiota show spatial variations in abundance and modulate the physiology of their host, which invites therapeutic targeting.

Keywords: Antimicrobial peptides, Bacteriophages, Hair growth, Metabolism, Microbiome

Journal of Investigative Dermatology (2024) 144, 1353–1367; doi:10.1016/j.jid.2023.11.006

INTRODUCTION

Hair follicles (HFs) represent an environmentally protected major microbial reservoir (Constantinou et al, 2021a; Harris-Tryon and Grice, 2022; Lousada et al, 2021). Indeed, human HF metagenomics shows colonization by bacteria, fungi, viruses, and mites (Claesen et al, 2020; Conwill et al, 2022; Hall et al, 2018; Ho et al, 2019; Ring et al, 2019; Zari et al, 2008), with *Staphylococcus*, *Cutibacterium*, *Streptococcus*, and *Malassezia* being predominant commensals (Hall et al, 2018; Ho et al, 2019). However, the intrafollicular distribution and composition of the human HF microbiota, as well as their viability and impact on HF functions remain underexplored. Given the known microbial impact on murine skin/HF development, regeneration, and inflammation, this constitutes a critical gap in our understanding of human skin physiology.

Traditional skin microbiota sampling methods (swabs, scrapings, skin biopsies, and plucking) fail to eliminate extra-follicular communities and/or have limited sampling depth, since they miss, for example, the hair matrix and mesenchyme (Lousada et al, 2021). Furthermore, HFs underlie important compartment-specific variations in mitochondrial and metabolic activity, oxygen and nutrient availability, and ROS production (Figlak et al, 2021; Lemasters et al, 2017; Li et al, 2019; Vidali et al, 2014) that must be considered in a HF microbiota context. Indeed, bacteriome variations have been reported between HF segments (Ho et al, 2019; Lousada et al, 2023). In addition, although age-dependent skin microbiota shifts are known (Kim et al, 2022; Williams et al, 2020; Wu et al, 2020), these remain to be explored in HFs. Shifts in microbiota composition are also observed in HF-associated diseases, including acne vulgaris, hidradenitis suppurativa, alopecia areata, androgenetic alopecia, and squamous cell carcinoma (Chopra et al, 2022; Constantinou et al, 2021b; Ho et al, 2019; O'Neill and Gallo, 2018; Pinto et al, 2019; Ring et al, 2019; Voigt et al, 2022). Hence, understanding functional microbiota–HF interactions is important to evaluate how dysbiosis contributes to disease development. Interestingly, antibiotic treatment–derived effects on human hair growth have been described (Ito et al, 2009; Bispo Lousada et al, 2021), suggesting that dysbiosis might directly affect human HF biology. This potential direct effect requires careful consideration, given that gut microbiota–derived metabolites are already known to alter gut epithelial barrier function, autophagy, cellular metabolism, and immune regulation (Fan and Pedersen, 2021; Kim, 2021; Larabi et al, 2020; Ratajczak et al, 2019).

¹Monasterium Laboratory, Münster, Germany; ²Zoological Institute, Christian Albrechts University in Kiel, Kiel, Germany; ³Dr Phillip Frost Department of Dermatology and Cutaneous Surgery, University of Miami Miller School of Medicine, Miami, Florida, USA; ⁴Mediteknia Skin & Hair Lab, Las Palmas de Gran Canaria, Spain; ⁵Ciencias de la Salud, Universidad Fernando Pessoa Canarias, Las Palmas de Gran Canaria, Spain; ⁶Hautarztpraxis Dr Pajouh, Bargteheide, Germany; and ⁷CUTANEON, Hamburg, Germany

Correspondence: Ralf Paus, Dr. Phillip Frost Department of Dermatology and Cutaneous Surgery, University of Miami Miller School of Medicine, 1600 NW 10th Avenue, RMSB, Room 2023A, Miami, Florida 33136, USA. E-mail: rpx803@med.miami.edu

Abbreviations: AMP, antimicrobial peptide; DP, dermal papilla; HF, hair follicle; LCM, laser-capture microdissection; PMA, propidium monoazide

Received 23 February 2023; revised 17 October 2023; accepted 1 November 2023; accepted manuscript published online 7 December 2023; corrected proof published online 23 February 2024

Therefore, this study aimed to comprehensively characterize regional, tissue lineage, viability, and donor age-dependent variations of the human HF-specific microbiota and to probe the functional impact of selected microbiota and some of their key metabolites on human scalp HF physiology *ex vivo*. For this, human scalp HFs were laser-capture microdissected into defined anatomical compartments and evaluated by metagenomic shotgun sequencing, whereas microbiota viability was tested by propidium monoazide (PMA) assay and ribosomal RNA FISH. In additional pilot studies, the microbiota's impact on human HF biology *ex vivo* was assessed by treating organ-cultured human scalp HFs with *Staphylococcus epidermidis*-specific lytic bacteriophages or butyrate, a key *S. epidermidis* metabolite.

RESULTS

Human scalp HFs exhibit age-, region-, and tissue lineage-specific variations in microbial abundance

To comprehensively characterize the physiological human HF-specific microbiota, scalp anagen HFs from 10 males were laser microdissected into 9 anatomically distinct compartments (Figure 1a) and metagenomic shotgun sequenced (Grogan et al, 2019).

Strong interindividual variations in alpha diversity ($P < .05$) (Supplementary Figure S1a) and beta diversity ($P \leq .001$) were observed, translating into significant donor age-dependent variations in beta diversity ($P < .001$). After controlling for these interindividual variations, significant differences in beta diversity were also found according to HF region ($P \leq .01$) and tissue lineage ($P \leq .001$) (Supplementary Figure S1b), demonstrating site-dependent differential commensal distribution.

Cutibacterium acnes and *Malassezia restricta* are the most abundant HF species also in the HF mesenchyme

As expected of sebaceous skin sites (Bouslimani et al, 2015; Byrd et al, 2018; Grice and Segre, 2011), bacteria accounted for 75.86% of the reads, with a predominance of *Actinobacteria*, *Proteobacteria*, and *Firmicutes*, while fungi represented 24.02% and viruses and archaea represented 0.12% (Supplementary Figure S2a–c).

Although strong interindividual abundance variations were detected (Supplementary Figure S3), *C. acnes* and *M. restricta* dominated the microbiota, being highest in younger donors and, surprisingly, in the mesenchyme (Figure 1b–f). Contrasting with previous reports (Grice and Segre, 2011; Pinto et al., 2019), *S. aureus* and *M. globosa* were not among the top 10 identified species (Figure 1b–d), whereas unexpectedly, *Mycobacterium* was (~5% of reads) (Figure 1b–d). However, the latter phenomenon might result from contamination artifacts from published eukaryotic genomes (Lu and Salzberg, 2018). Higher microbial load of the top identified species was also detected in the HF mesenchyme, particularly in the dermal papilla (DP) as well as in the suprabulbar and isthmus regions of the dermal sheath, mainly driven by *C. acnes* and *M. restricta* abundance (Figure 1b–f). Interestingly, among the less numerous species, *S. epidermidis* abundance varied most between compartments, being highest in the suprabulbar and isthmus regions (Figure 1g). Regional viral and archaeal variations were also found, with highest abundance of the most predominant species in the epithelium. Although only Papillomaviruses,

Dependoviruses, Adeno-associated viruses, and *Propionibacterium* phages were previously reported as human HF commensals (Lousada et al, 2021), in this study also, *Pseudomonas* and *Faecalibacterium* phages and *Gammaretrovirus* murine leukemia virus were identified (Supplementary Figure S4). Although no HF-specific archaeal evaluation was conducted to date, this study identified *Halomicrobium*, *Halopenitus*, *Natromonas*, and *Nitrosopumilus* as HF microbiota constituents, along with *Halosimplex*, *Methanobrevibacter*, and *Saccharolobus*, previously noted in the skin microbiome (Probst et al, 2013; Umbach et al, 2021) (Supplementary Figure S4 and Supplementary Text S1).

These findings suggest that the compartmentalized oxygen level, nutrient supply, metabolism, immune cell composition, and antimicrobial peptide (AMP) production differences (Bertolini et al, 2020; Chéret et al, 2018; Christoph et al, 2000; Emelianov et al, 2012; Polak-Witka et al, 2021, 2020; Purba et al, 2021; Reithmayer et al, 2009; Wu et al, 2009) translate into species abundance variations. Thus, similar to the epidermal environment (Flowers and Grice, 2020; Harris-Tryon and Grice, 2022), defined HF compartments appear to differ in how they favor microbial survival.

C. acnes and *M. restricta* represent the most abundant viable human scalp HF colonizers, and the functional evaluation of the HF microbiota mirrors the region-, tissue lineage-, and donor age-specific differences

In a pilot study with two donors, PMA was added to the samples prior to DNA extraction to assess microbial viability (Lu et al, 2018) (Supplementary Text S2), this resulted in significantly reduced microbial abundance compared with untreated controls ($P \leq .001$). PMA sequencing highlighted interindividual species' abundance variations and accentuated regional abundance differences ($P \leq .05$) (Figure 2a), with no reads detected in the suprabulbar region of these two donors (Figure 2a). Significant tissue lineage ($P \leq .05$) variations were also observed after PMA treatment, with a higher load of the most abundant bacteria and fungi observed in the PMA-treated HF epithelium (Figure 2b). This preliminary sequencing data in two donors might suggest that the HF epithelium offers easier access for viable microbial colonization and/or that these microbes find here more favorable growth conditions.

Taxonomical characterization showed no PMA influence on total microbial abundance (Supplementary Figure S5), with *C. acnes* and *M. restricta* remaining among the most abundant species (Figure 2). Identification of *Sphingomonas* and *Acinetobacter* was also possible; however, given that these were amplified only after PMA treatment and are associated with contaminants from DNA extraction reagents, their presence requires further evaluation (Salter et al, 2014). Interestingly, after PMA, there was a shift in the abundance of *C. acnes*, *M. restricta*, and *S. epidermidis*, showing a higher abundance of these in the DP, infundibulum, and epithelial tissues (Figure 2c–e).

To visualize 2 core viable HF bacteria with the highest predominance and variability between regions (*C. acnes* and *S. epidermidis*), FISH of human HFs was conducted with the eubacterial 16S, *C. acnes*-, and *S. epidermidis*-specific probes. Bacteria were ubiquitously distributed, yet showed

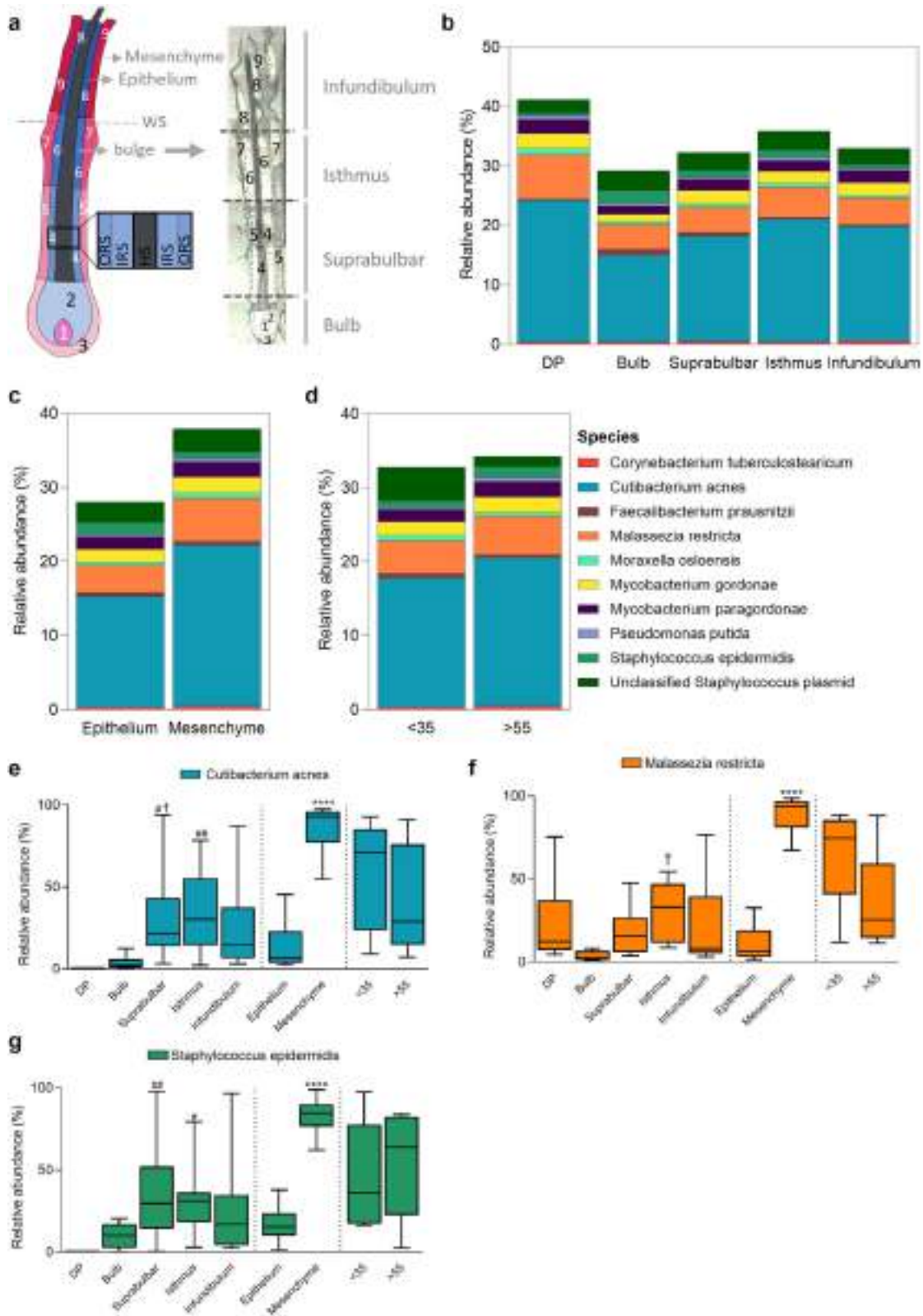
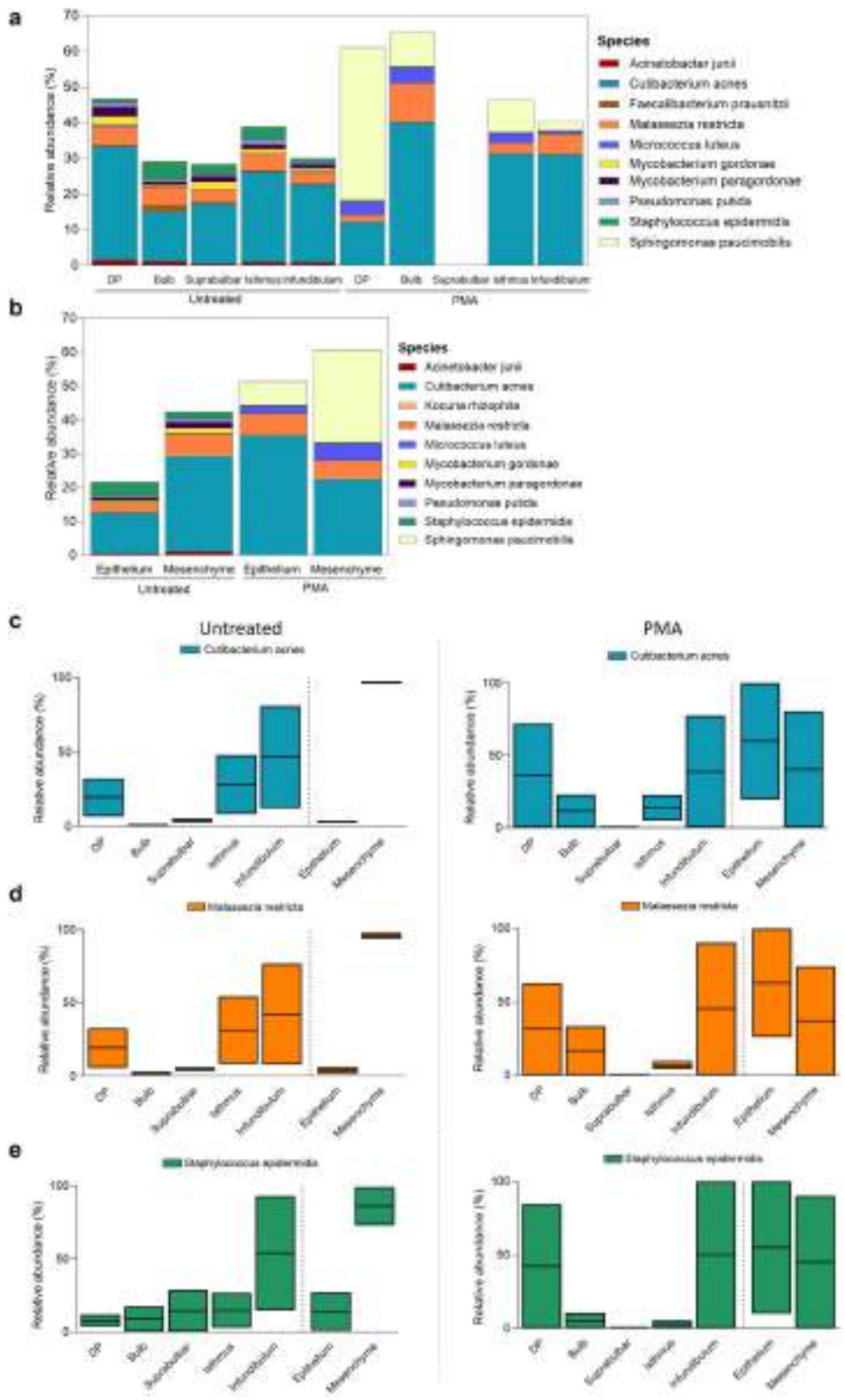


Figure 1. Human HF microbiota vary between HF regions, tissue lineage, and donors of different age. (a) Representative scheme of the nine anatomical divisions of the HF separated with LCM (left) and respective laser cuts as seen under the LCM microscope (right). Divided areas are as follows: (1) dermal papilla, (2) epithelial bulb tissue, (3) mesenchymal bulb tissue, (4) epithelial suprabulbar tissue, (5) mesenchymal suprabulbar tissue, (6) epithelial isthmus tissue, (7) mesenchymal isthmus tissue, (8) epithelial infundibulum tissue, and (9) mesenchymal infundibulum tissue. Shotgun metagenomic sequencing of healthy unmanipulated HFs after LCM was performed. Relative abundance of the top 10 main bacterial and fungal species found in the HF compared between (b) each of the 5 HF anatomically distinct regions, (c) the 2 main HF tissue lineages, and (d) donor age group is shown. Note that the unclassified *Staphylococcus* plasmid was identified by BLAST search and this identification is shown in [Supplementary Table S5](#). Relative abundance of 3 selected HF microbiota species—(e) *Cutibacterium acnes*, (f) *Malassezia restricta*, and (g) *Staphylococcus epidermidis*—per HF region, tissue lineage, and donor age group is shown. Data pooled

Figure 2. PMA treatment limits HF microbiota abundance and conserves regional and tissue-lineage variations.

PMA shotgun metagenomic sequencing of healthy unmanipulated HF after LCM was performed. Relative abundance of the top 10 main bacterial and fungal species in (a) 5 anatomically distinct HF regions and (b) the 2 main tissue lineages found in the HF is shown. Interestingly, PMA treatment depleted the HF bacterial and fungal reads in the suprabulbar area. Relative abundance of 3 selected HF microbiota species before (left) and after (right) PMA treatment—(c) *Cutibacterium acnes*, (d) *Malassezia restricta*, and (e) *Staphylococcus epidermidis*—per HF region and tissue lineage is shown. Data pooled from n = 2 donors, corresponding to n = 5 HFs per donor, are represented as mean ± SEM. D’Agostino and Pearson omnibus normality test, no Gaussian distribution, and Mann–Whitney test, n.s., were performed. DP, dermal papilla; HF, hair follicle; LCM, laser-capture microdissection; n.s., not significant; PMA, propidium monoazide.



from n = 10 donors (for b, c, and e–g) or n = 5 donors each (for d), corresponding to n = 5 HFs per donor, are represented as mean ± SEM. D’Agostino and Pearson omnibus normality test, Gaussian distribution, and ordinary 1-way ANOVA were performed; #/†P < .05, ##/†P < .01, and ****P < .0001. # denotes a significant difference from the DP; † denotes a significant difference from the bulb, and * denotes a significant difference from the epithelium. BLAST, Basic Local Alignment Search Tool; DP, dermal papilla; HF, hair follicle; HS, hair shaft; IRS, inner root sheath; LCM, laser-capture microdissection; ORS, outer root sheath; WS, immunological watershed.

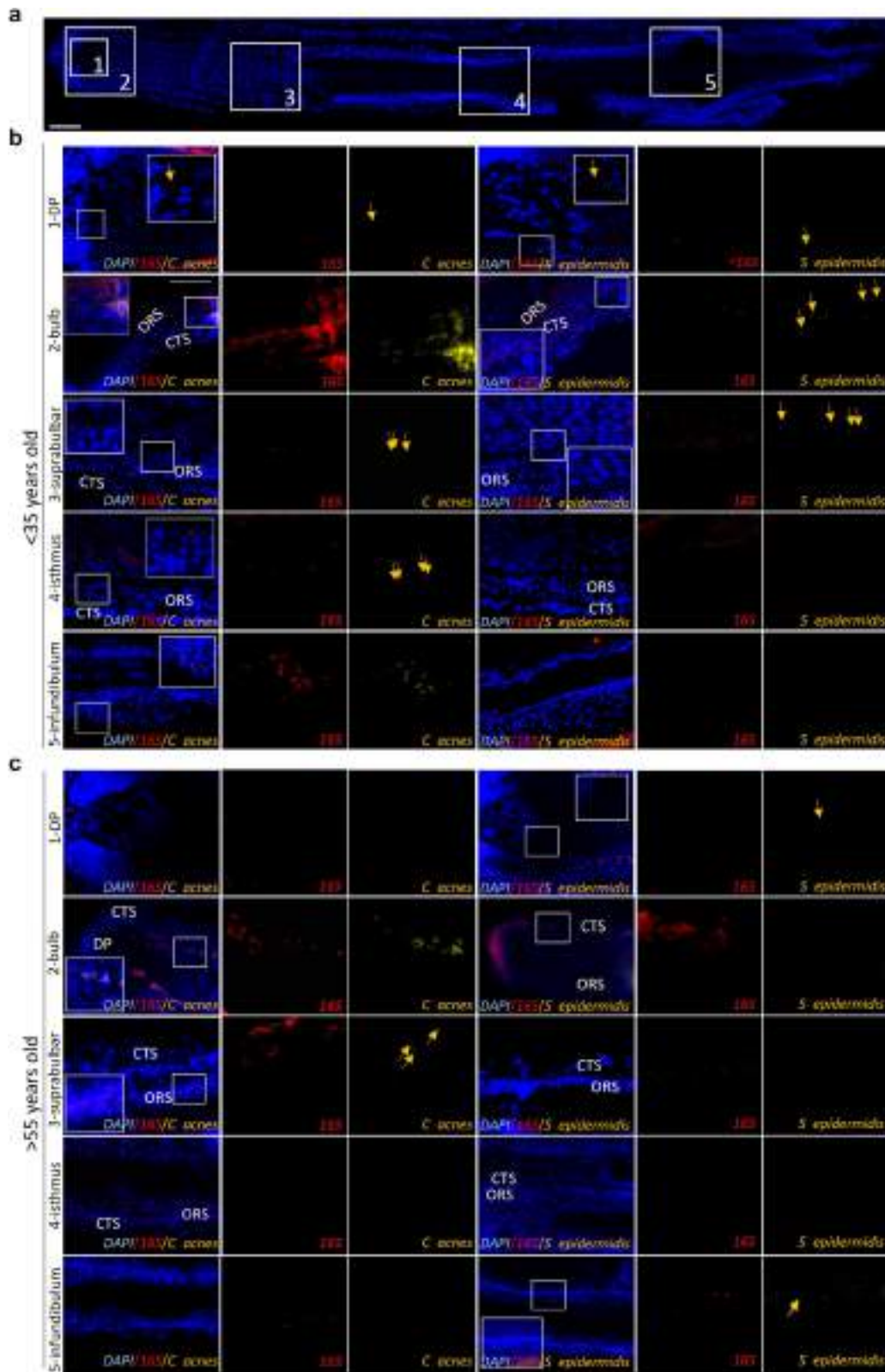


Figure 3. Representative FISH visualization of *C. acnes* and *S. epidermidis* in 5 areas of the scalp HF per donor age group. (a) Representative image showcasing the four HF areas where FISH was imaged, namely: (1) DP, (2) bulb, (3) suprabulbar, (4) isthmus, and (5) infundibulum. FISH analysis of healthy unmanipulated and freshly frozen HFs in a (b) donor aged <35 years and (c) donor aged >55 years, with the 16S eubacterial probe (red) and *C. acnes*–(left) or *S. epidermidis*–specific (right) probes (Supplementary Table S2), was performed. Nuclei are counterstained with DAPI (blue). Single-channel images display high magnification inserts of the areas marked with white rectangles where double-positive dots could be found. Yellow arrows demark those double-positive dots, indicating the presence of *C. acnes* (left) or *S. epidermidis* (right). Bar = 100 μ m. CTS, connective tissue sheath; DP, dermal papilla; HF, hair follicle; ORS, outer root sheath.

the highest load in the bulb (Figure 3b2 and c2) and distal HF (Figure 3b4, b5, c4, and c5). While *C. acnes* was ubiquitous (Figure 3b and c), *S. epidermidis* was visualized mostly in the bulb/suprabulbar and infundibulum regions (Figure 3b and c). These findings support previous studies emphasizing *C. acnes*, *S. epidermidis*, and *M. restricta* as main human HF microbiota therapeutic targets (Fournière et al, 2020; Jo et al, 2022; Park et al, 2018). Contrasting with the sequencing data, FISH showed that total bacterial load (16S rRNA) within the DP was low, yet confirmed a similar abundance of *S. epidermidis* and *C. acnes* in this region of the HF (Figure 3b1 and c1). This could result from the error associated with metagenomic analysis of low biomass compartments (Liu et al, 2022), such as the DP, or from the differential methodology used. Also, while metagenomic shotgun sequencing was generated from 5 complete full-length HFs per donor, FISH was imaged only in single HF sections per donor.

After viability analysis, the human HF microbiota functional profile was also evaluated, by metagenomic shotgun sequencing, revealing significant differences between regions ($P \leq .001$), tissue lineage ($P \leq .001$), and donor age group ($P \leq .001$). Interestingly, the microbiota of the suprabulbar and isthmus regions, mesenchyme, and younger donors exhibited the highest gene content related to carbohydrate, amino acid, vitamin, pigment, metabolic cofactor, RNA and protein metabolism, and virulence (Supplementary Figure S6a). After PMA treatment, regional and tissue lineage differences in the enriched pathways were also found ($P \leq .01$) (Supplementary Figure S6b). Notably, this analysis with PMA treatment found highest gene content related to the above-mentioned pathways, in addition to fatty acid and lipid metabolism found in the DP (Supplementary Figure S6a), the HF's mesenchymal command center (Abreu et al, 2020; Andl et al, 2023; Geyfman et al, 2015; Paus and Cotsarelis, 1999; Schneider et al, 2009).

Targeted restriction of *S. epidermidis* abundance manipulates human HF transcriptional profile

To probe the functional impact of selected microbiota on human HF biology, HF organ cultures were infected with *S. epidermidis*-specific (*SEPI*) bacteriophages (Melo et al, 2014). This successfully depleted *S. epidermidis* in 3 of 4 samples and increased total bacterial load in 2 of 4 samples, as assessed by RT-qPCR (Figure 4a and b). Given the known ecological interactions between *S. epidermidis*, *C. acnes*, and *S. aureus* (Supplementary Text S3), skin/HF microbiota identified in dysbiosis-associated HF diseases (Fournière et al, 2020; Tsuru et al, 2021), the indirect *SEPI* effects on the latter bacteria were also evaluated. This revealed *C. acnes* reduction in all samples and *S. aureus* increase in 2 of 4 samples (Figure 4b), suggesting both microbe-microbe regulation and baseline microbiota interindividual variations (Supplementary Text S3).

HF transcriptomic profiling of this bacteriophage-induced dysbiosis by RNA sequencing revealed modulation of 923 intrafollicularly transcribed genes compared with those of unmanipulated controls (denoted as D0) and 843 differentially regulated genes in D0 versus those in vehicle-treated HFs (Figure 4c and d). Comparison of *SEPI* treatment-specific versus vehicle-regulated transcripts showed upregulation of

immune regulatory genes, including *MRC1* (in 2 of 4 donors), *CD274*, *IL1R2*, *IRAK2*, *RNF125*, and *PIK3CD* (Supplementary Figure S7a and b) (Arimoto et al, 2007; Cannons et al, 2021; Castillo et al, 2021; Kuninaka et al, 2022; Pilkington et al, 2018; Sibaud, 2018). Subsequent enrichment analyses of *SEPI*-regulated genes (Figure 4c, pink) indicated significant HF growth and development; melanogenesis; lipid, glucose, and carbohydrate metabolism; and mitochondrial function transcription modulation (Figure 4e and f). Namely, HF growth-promoting genes were downregulated after *SEPI*, such as *PLCB2*, *SOSTDC1*, *LTBP2*, *LGR5*, *FGF18*, *CNR1*, and *ITGA6* (Bodó et al, 2007; Kawano et al, 2005; Polkoff et al, 2022; Rittié et al, 2009; Yoon and Detmar, 2022), with upregulation of growth and development inhibitors, including *KREMEN2*, *PTGS1*, serpins, *SOX11*, and *PYGL* (Figlak et al, 2021; Garza et al, 2012; Jensen et al, 2000; Miao et al, 2019; Zhu et al, 2020) (Figure 4g). Reduced mitochondrial activity and melanogenesis gene transcription were also seen, namely in *SLC25A34*, *SCL25A35*, *DCT*, and *POMC* (Figure 4g and h) (Ng et al, 2022; Slominski et al, 2000; Tiede et al, 2021), together with upregulation of mitophagy and ROS clearance genes, that is, *BNIP2L* and *SOD2* (Figure 4h) (Li et al, 2021; Tang et al, 2016).

Immunohistochemistry and immunofluorescence analysis of anagen VI HFs after *SEPI* treatment for 2 days (Supplementary Figure S7c–e) surprisingly showed a tendential decrease in hair matrix keratinocyte autophagic flux, as evaluated by LC3b expression (Supplementary Figure S7f and g). During the short HF organ cultured period used, which was selected due to the progressive tissue damage resulting from microbial overgrowth when antibiotics are omitted from the culture medium (Bispo Lousada et al, 2021; Edelkamp et al., 2023), no changes in mitochondrial activity and melanogenesis were seen, as quantitatively evaluated by MTCO1 and gp100 protein expression (Supplementary Figure S7h–k) and melanin histochemistry (Supplementary Figure S7l and m). Notably, previous studies have assessed intrafollicular protein expression after 6–7 days of culture (Nicu et al, 2021; Suzuki et al, 2023). Therefore, although validation is necessary, these modifications suggest that *S. epidermidis* depletion and/or consequential dysbiosis alter the gene expression profile and autophagic flux of human scalp HFs.

Butyrate treatment delays catagen progression and stimulates intrafollicular melanosome production ex vivo

Considering the transcriptional changes observed after *SEPI* treatment, to further explore the effects of the HF microbiota and their metabolites on hair biology, organ cultured human scalp HFs were treated with butyrate. Butyrate is a HF microbiota-derived metabolite, produced by various members of the identified HF microbiota (Supplementary Text S4), including *S. epidermidis* (Traisaeng et al, 2019), one of the top 10 and more variable species between HF regions (Figure 1g). In addition, this metabolite is known to impact on lipid and glucose metabolism, mitochondrial function, and autophagy (Hu et al., 2020; Zhang et al., 2021, 2022). This is important in the current context since these are determinants of anagen duration (Figlak et al., 2021; Parodi et al., 2018) (Supplementary Text S4).

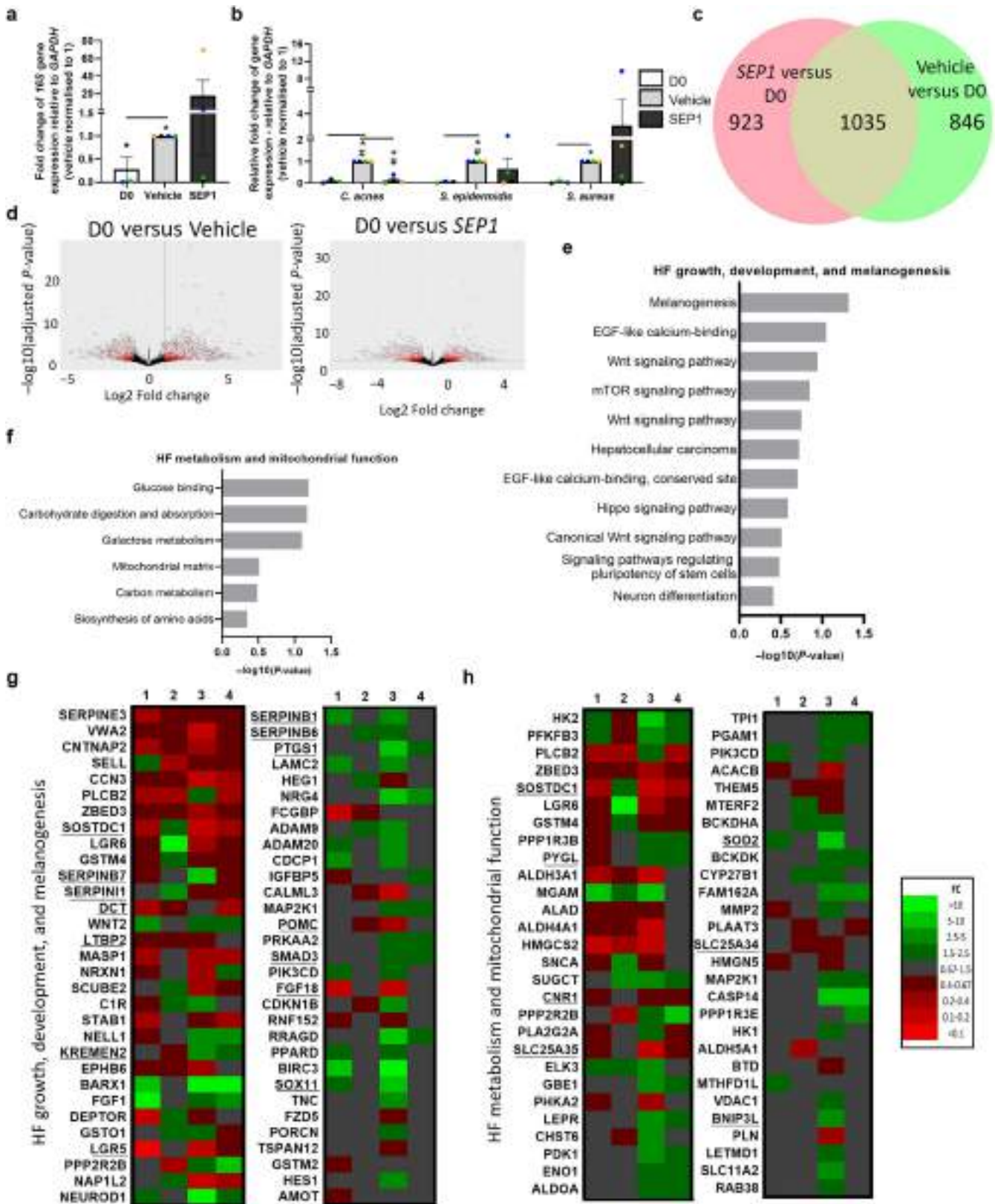


Figure 4. Restriction of *S. epidermidis* growth with *SEPI* bacteriophage treatment regulates several HF growth, development, melanogenesis; lipid, glucose, and carbohydrate metabolism; and mitochondrial function genes. Healthy microdissected HFs were cultured in the absence of antibiotics and the presence of SM buffer (vehicle) or *SEPI* bacteriophages and evaluated by RT-qPCR and RNA sequencing after 30 h of bacteriophage infection. Relative fold change of the (a) *16S* gene and (b) *C. acnes*-, *S. epidermidis*-, and *S. aureus*-specific genes after *SEPI* treatment, as analyzed by RT-qPCR. Data from technical triplicates, corresponding to $n = 4$ donors, and to $n = 2$ HFs per donor, are represented as mean \pm SEM. D'Agostino and Pearson omnibus normality test, no Gaussian distribution, Kruskal–Wallis test, and Dunn's multiple comparison test ($\#P < .05$) and Mann–Whitney test ($*P < .05$) were performed compared with the vehicle. Symbol colors represent the different individuals. (c) Euler diagram showing the number of significantly regulated genes between the vehicle control

Butyrate significantly decreased the percentage of mid-catagen HF, thus delaying catagen progression (Figure 5a–c), as confirmed by a significantly lower hair cycle score (Figure 5b). However, keratinocyte proliferation in the hair matrix was unaffected (Supplementary Figure S8a and b). Given the *SEP1* treatment effects on melanogenesis, HF pigmentation after butyrate was also evaluated (O’Sullivan et al, 2021). This showed significantly increased gp100 protein expression within the HF pigmentary unit (Figure 5d and e), suggesting increased melanosome production (Hardman et al, 2015; O’Sullivan et al, 2021; Sevilla et al, 2023), while no changes in HF melanin synthesis were detectable during this short culture period (Supplementary Figure S8c–d).

Butyrate may promote intrafollicular autophagy, mitochondrial activity, and AMP production

Given the importance of metabolism, mitochondrial function, and autophagy for HF growth (Chai et al, 2019; Figlak et al, 2021; Lemasters et al, 2017; Parodi et al, 2018; Vidali et al, 2014) and the impact of *SEP1* treatment, the effects of butyrate on these were explored by quantitative immunohistochemistry. Butyrate significantly increased the number of LC3b+ autophagosomes (Figure 5f and g) and mitochondrial function, as measured by MTCO1 protein expression, a read-out parameter that correlates well with TFAM and PGC1 α expression and mitochondrial activity in human HF (Vidali et al, 2016, 2014) (Figure 5h and i).

Finally, to probe how butyrate impacts intrafollicular AMP production and thereby HF microbiota management, the expression of 3 key intrafollicular AMPs—dermcidin (*DCD*), psoriasin (*S100A7*), and LL-37 (*CAMP*) (Chéret et al, 2018; Emelianov et al, 2012; Yao et al, 2022)—was assessed. While no changes in *S100A7* and *CAMP* expression were observed (Supplementary Figure S8e), butyrate increased *DCD* mRNA and significantly increased its protein expression (Figure 5j–l).

Hence, this key *S. epidermidis* metabolite appears to alter selected human HF functions *ex vivo*, namely HF cycling, premelanosome synthesis, mitochondrial function, autophagy, and dermcidin production.

DISCUSSION

By combining LCM, metagenomic shotgun sequencing, and PMA assays, this study reveals significant HF microbiota abundance and viability variations on the basis of HF compartment, tissue lineage, and donor age. This approach revealed that, unexpectedly, the most predominant microbial species show the highest abundance within the HF mesenchyme, driven by *C. acnes* and *M. restricta*, which are also the most abundant viable species. *S. epidermidis* abundance

showed great variations between HF compartments, suggesting that these colonizers are sensitive to compartmentalized habitat fluctuations, finding optimal growth conditions in the hair bulb and distal epithelium. Functionally, this pilot data on the modulation of HF gene transcription by *S. epidermidis*-specific lytic bacteriophages indicate a downregulation of genes involved in the control of HF growth and development, metabolism, and melanogenesis. Likewise, that butyrate treatment may promote intrafollicular autophagy and mitochondrial function and stimulate intrafollicular dermcidin production. These findings suggest that the observed variations in HF microbiota distribution may translate into functional changes via differences in microbial metabolite production within distinct HF compartments.

Although this study provides the most comprehensive analysis of human scalp HF microbiota available to date, the overall taxonomic profile found is similar to previous reports (Bouslimani et al, 2015; Hall et al, 2018; Ho et al, 2019; Pinto et al, 2019; Ring et al, 2019), confirming *C. acnes*, *M. restricta*, and *Propionibacterium* phages predominance in human scalp/HF microbiota (Hall et al, 2018; James et al, 2013). In addition, this study analyzed the HF-specific archaeal communities, demonstrating the presence of halophiles and methanogens (Probst et al, 2013). However, their presence and function remain to be confirmed, given their low biomass, which represents a study limitation (Supplementary Text S5), the limited available databases, and since these findings might constitute a transient environmental layer (Umbach et al, 2021).

Furthermore, in contrast to previous reports, which likely also have sampled skin surface and extrafollicular microbiota (Hall et al, 2018; Pinto et al, 2019), our HF-specific sampling methodology revealed a striking absence of *S. aureus* and *M. globosa* among the top 10 species identified. That a high load of the top identified species was also found in the mesenchyme of untreated samples also contrasts with previous evaluations that had suggested maximal microbial load in the distal HF epithelium (Polak-Witka et al, 2021). Instead, our PMA treatment results from HF of two donors correspond with the latter study, which nevertheless had methodologically missed sampling of the proximal HF and/or did not compare tissue lineages. Although other evaluations (Alexeyev et al, 2012; Jahns and Alexeyev, 2014) also did not distinguish lineages, interestingly, a *C. acnes* invasion analysis of hidradenitis suppurativa samples showed mesenchymal and dermal tissue invasion, with lower detection of these bacteria in the epithelium (Jahns et al, 2014). Yet, given that our study could analyze only 10 donors and the PMA treatment was performed only on two donors, quantitative analyses in additional donors comparing the microbiota

(right) or *SEP1* bacteriophage (left) treatment with control healthy untreated HF (denoted as D0). The further analyzed genes correspond to the left of the diagram (pink), meaning those genes regulated only after treatment with *SEP1* bacteriophages. (d) Volcano plots with the log₂FC of the *P*-adjusted value of the differentially regulated genes between the vehicle control and the D0 control (left) and between the *SEP1* bacteriophage treatment and the D0 control (right). Lines indicate 1 and -1 log₂FC values and *P*-adjusted value significance. (e, f) Significantly enriched gene clusters and respective *P*-adjusted values found by GO, KEGG pathway, and functional annotation analysis cluster with the DAVID online tool (Sherman et al, 2022) in (e) HF growth, development, and melanogenesis and (f) metabolism and mitochondrial function clusters. Heat map comparison between the *SEP1* treatment and vehicle control displaying the regulated genes within each GO analysis cluster per individual (1–4)—(g) HF growth, development, and melanogenesis and (h) metabolism and mitochondrial function clusters—is shown. Underlined genes in each heatmap correspond to genes mentioned in the text. Data are from *n* = 4 donors, corresponding to *n* = 2 HF per donor. GO, Gene Ontology; h, hour; HF, hair follicle; KEGG, Kyoto Encyclopedia of Genes and Genomes; log₂FC, log₂ fold change.

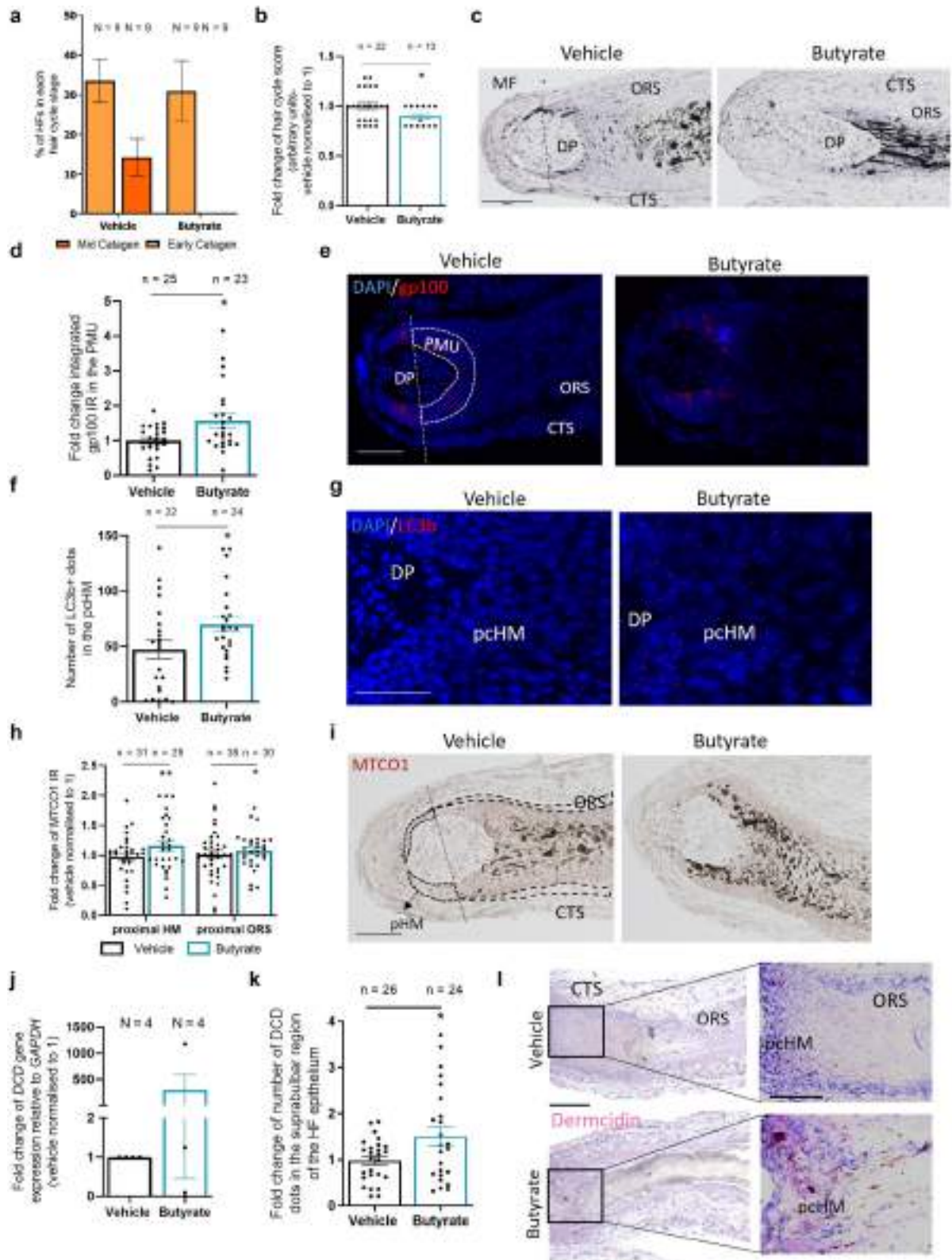


Figure 5. Butyrate delays catagen progression and significantly promotes gp100, LC3b, MTCO1, and DCD protein expression *ex vivo*. Healthy microdissected HF were cultured for 7–8 days in the presence of antibiotics, with William complete medium (vehicle) or 1 mM butyrate. **(a)** Percentage of catagen HF, as staged on the basis of MF histochemistry and Ki-67/TUNEL immunofluorescence, and **(b)** hair cycle score (in arbitrary units: 200 [early catagen] and 300 [mid-catagen]). Pooled data are from $n = 9$ donors, corresponding to $n = 13$ – 22 full-length and amputated catagen HF. **(c)** Representative MF histochemistry images. Bar = 100 μm . **(d)** Integrated gp100 immunoreactivity in the pigmentary unit of anagen VI HF and **(e)** respective representative images, with delineated area of analysis. **(f)** Number of LC3b dots within the pCHM of anagen VI HF and **(g)** respective representative images. **(h)** MTCO1 immunohistochemistry in the pCHM and ORS of anagen VI HF (in selected donors) and **(i)** respective representative images, with indication of the areas analyzed. **(j)** *DCD* gene expression changes after 24 h of butyrate treatment, with donor-dependent effects. Data are from $n = 4$ donors. **(k)** *DCD* protein expression in the HF suprabulbar region

distribution of the HF mesenchyme with epithelium and between proximal and distal HF compartments are needed for definitive characterization of the human scalp HF microbiota. If confirmed, the higher *C. acnes* abundance in the proximal mesenchyme might indicate, for example, a role in HF mesenchymal stem cell proliferation and migration, as observed in the human gut and bone marrow (Markandey et al, 2021; Silveira et al, 2019). Furthermore, because HFs often display *C. acnes* biofilms (Jahns and Alexeyev, 2014), it is possible that the HF mesenchyme facilitates biofilm formation, as reported in *C. acnes* infection of bone marrow—derived mesenchymal stem cells (Dubus et al, 2022; El-Mahdy et al, 2021; Jahns and Alexeyev, 2014). HF infection with *C. acnes*—specific bacteriophages could interrogate the impact of these bacteria on the inductive properties of the HF mesenchyme, as measured by changes in the activity/expression of key DP morphogens, such as, versican, noggin, and hepatocyte GF (Geyfman et al, 2015; Paus and Foitzik, 2004; Schneider et al, 2009).

The differential distribution of HF microbiota abundance observed herein may reflect compartment-specific metabolic and nutritional variations (Figlak et al, 2021; Purba et al, 2021; Williams et al, 2020) but also age-related environment alterations in the HF (Supplementary Text S6) as well as immunologically distinct HF habitats (Bertolini et al, 2020; Purba et al, 2021). The HF mesenchyme offers greater proximity to the dermal white adipose tissue and blood vessels than the epithelium, thereby offering a lipid-rich environment with higher oxygen levels (Kruglikov et al, 2022; Nicu et al, 2021; Poblet et al, 2018). This could shape the microbiota according to their nutritional and oxygen dependencies. In addition, the human HF epithelium abundantly generates AMPs (Chéret et al, 2018; Emelianov et al, 2012; Reithmayer et al, 2009; Yao et al, 2022), is rich in free radical-producing mitochondria (Lemasters et al, 2017; Vidali et al, 2014), and is distally populated by functional Langerhans and T cells. Contrarily, the HF mesenchyme appears to generate fewer AMPs, is mitochondria poor, and is mainly populated by mast cells and macrophages (Bertolini et al, 2014; Christoph et al, 2000; Hardman et al, 2019). These major functional differences must impact microbial distribution, abundance, viability, and secretory activities. Hence, it deserves exploration whether the predicted microbial metabolic functions, which may directly influence HF biology (Supplementary Figure S6), at least potentiate compartmentalized metabolic differences (Figlak et al, 2021; Purba et al, 2021). Indeed, characterization of the skin surface microbiota and their potential metabolites suggests that these microbes alter the chemical composition of the skin microenvironment. For example, the variation in *Propionibacteria* might directly correlate with the levels of oleic acid (Bouslimani et al, 2015).

The limited viability of healthy human scalp microbiota found by PMA assay (Supplementary Text S2) is

independently supported by ribosomal RNA FISH data, which confirmed the PMA-induced reduction of the bacterial load. Although the human scalp HF mycobiota warrants stricter evaluation, our viability data support that *C. acnes*, *S. epidermidis*, and *M. restricta* are the most significant therapeutic targets among viable microbiota. This is clinically relevant because their dysbiosis is associated with acne vulgaris, hidradenitis suppurativa, dandruff, and alopecia areata (Lousada et al, 2021; Polak-Witka et al, 2020; Rinaldi et al., 2022).

Although these functional pilot data are preliminary, the modulation of the human HF transcriptional profile and LC3b protein expression by *S. epidermidis*—selective bacteriophage treatment suggest that a) individual changes in the HF microbiota abundance could indeed impact human HF physiology, and b) that the selective manipulation of human HF microbiota is feasible in principle, at least *ex vivo*. Similarly, if follow-up studies confirm that defined HF microbiota metabolites, such as butyrate, stimulate intra-follicular autophagic flux, mitochondrial activity, melanosome, and/or AMP production, the application of selected microbial-derived short-chain fatty acids deserves exploration as a strategy for the management of HF-associated dermatoses where any of these is defective. Given the similar effects that both *SEPI* bacteriophage and butyrate treatment exert on the intrafollicular mRNA and protein expression profile, it might be hypothesized that butyrate reduction is the mechanism of action that underlies the observed effects of *S. epidermidis* growth restriction; this requires confirmation, for example, by biochemical measurement of butyrate levels and lipidomic profiling. Hence, although these preliminary data already suggest that manipulation of the human HF microbiota might be therapeutically relevant, they only provide a starting point for systematic follow-up studies that generate mechanistic insights.

MATERIALS AND METHODS

Human HF collection

This research was conducted according to the Declaration of Helsinki principles. Scalp anagen VI HFs were obtained from routine hair transplantation or facelift surgery after informed, written patient consent and ethics committee approval from the Comité de Bioética de la Universidad Fernando Pessoa Canarias (03 (2020-06-22)) and the Monasterium Laboratory Biobank (University of Muenster 2019-297-f-S, study plan 2020-954-f-S) (donor information is presented in Supplementary Table S1). Scalp HFs were directly embedded in optimal cutting temperature cryomatrix to preserve the *in vivo* microbiota (LCM-coupled metagenomics) or processed for *SEPI* or butyrate treatment in organ culture.

LCM, PMA treatment, and DNA extraction

LCM from 10 donors (5 HFs per donor) was performed as previously described (Lousada et al, 2023) on a contactless LCM system and without histological processing. Briefly, optimal cutting temperature compound—embedded samples were cryosectioned (10 μ m) and

after 7–8 days of *ex vivo* HF culture (from $n = 6$ donors) and (l) respective representative images. Data are represented as mean \pm SEM. D'Agostino and Pearson omnibus normality test, if data followed Gaussian distribution, and unpaired *t*-test (for **f**, **h**, and **k**) ($*P < .05$ and $**P < 0.01$) and Mann–Whitney test (for **a**, **b**, and **d**) ($*P < .05$), if data did not follow Gaussian distribution, were performed. CTS, connective tissue sheath; DP, dermal papilla; h, hour; HF, hair follicle; MF, Masson–Fontana; ORS, outer root sheath; pCHM, precortical hair matrix; pHc, proximal hair matrix; PMU, pigmentary unit.

further laser-capture microdissected into 9 compartments (Figure 1a) with a PALM MicroBeam (Zeiss) and the associated PALM Robo software (Zeiss). After LCM, additional samples from 2 donors (Supplementary Table S1) were treated with PMA to probe microbial viability, as described by Wang et al (2021). DNA was extracted with the SmartExtract DNA kit (Eurogentec), according to the manufacturer's instructions, followed by ethanol precipitation. Negative control samples were generated by LCM of tissue-free areas of optimal cutting temperature compound, whereas positive control samples were generated by the addition of a known plasmid to the extracted DNA of laser-microdissected samples from a randomly chosen donor (data not shown). In addition, during sequencing and library preparations, DNA- and DNase-free water controls were further carried out and excluded after sequencing, given the absence of reads.

Shotgun metagenomic sequencing and bioinformatic analysis

Precipitated DNA samples were shotgun sequenced at CosmosID Metagenomics Cloud (app.cosmosid.com), CosmosID (www.cosmosid.com). Before sequencing, DNA sample concentrations were measured by Qubit Assay (detection range of 0.1–120 ng). Given that some samples and negative controls were found to be below the assay threshold of detection (Supplementary Table S2), all samples were processed for sequencing. Libraries were constructed with a modified Illumina Nextera XT library preparation kit protocol and sequenced with an Illumina HiSeq 2 × 150 bp (20 M reads) (Grogan et al, 2019). Reads were processed with the Sunbeam pipeline; quality was evaluated using FastQC (version 0.11.5; Babraham Bioinformatics). Raw sequences are deposited on the Sequence Read Archive database under accession numbers PRJNA937066 and PRJNA937065. Adapter removal and trimming were done with cutadapt, version 2.6 (Martin, 2011), and Trimmomatic, version 0.36 (Bolger et al, 2014), with custom parameters (LEADING:3 TRAILING:3 SLIDINGWINDOW:4:15 MINLEN:36). Low-complexity sequences were detected with Komplexity, version 0.3.6 (Clarke et al, 2019). High-quality reads were mapped to the SEED database through translated homology search or the GRCh37, and those with 50% similarity across 60% of the read length were removed. The remaining reads were classified with Kraken2 and PlusPF database from 2021-05-17 (Wood et al, 2019) or annotated to Subsystems using Super-Focus (Silva et al, 2016). Samples with <500 counts assigned were filtered, and sample differences were accounted for by selection of random subsample to 500 counts.

Alpha diversity was measured using the Shannon diversity index, and beta diversity was measured using Bray–Curtis dissimilarities. Differences were evaluated with the nonparametric *t*-test, Kruskal–Wallis test, nonparametric ANOVA, and Scheirer–Ray–Hare test. Permutational multivariate ANOVA testing was used to identify the differences between the analyzed HF regions. Bray–Curtis dissimilarities distances between donors were compared, and, owing and in order to account for the high interindividual variability, a regression analysis of the donor identification was performed, assuming these as categorical variables. Another regression analysis was performed on the remaining identified variability using the different variables of interest (age, region, and tissue lineage) as the explanatory variable. For quality control, a second bioinformatic analysis, with the removal of the negative control samples as threshold was performed

(data not shown). Given the high degree of similarities, the direct approach was chosen for displayed.

FISH visualization

FISH was performed using the RNAscope Multiplex kit (Advanced Cell Diagnostics), following the manufacturer's instructions (probe details are provided in Supplementary Table S3).

Human HF organ culture (*SEPI* bacteriophage or butyrate treatment)

Human anagen VI HFs were microdissected as described elsewhere (Edelkamp et al, 2020), cultured in Williams complete medium and treated with 10⁸ plaque-forming unit/ml *SEPI* bacteriophage suspension, SM buffer, or 1 mM sodium butyrate (Supplementary Text S4). Bacteriophage suspensions were obtained from the Universidade do Minho (Melo et al, 2020, 2018) and propagated as described in Melo et al (2014). Bacteriophage infectivity was tested by spot assays and quantified by plaque assays. HF *SEPI* bacteriophage (Melo et al, 2018, 2014) or SM buffer (vehicle) treatment was done 24 hours after HF culture without antibiotics (Langan et al, 2015), and collection for RNA extraction was done 30 hours after infection for RNA sequencing and after 2–3 days (according to the amount of microbial growth (Bispo Lousada et al, 2021; Edelkamp et al., 2023) for protein expression analysis. Control healthy unmanipulated HFs (denoted as D0) were collected for RNA extraction prior to culture. Sodium butyrate (Sigma-Aldrich) treatment (Häselbarth et al, 2020; Schwarz et al, 2017) was done in media with antibiotics (penicillin/streptomycin mix, Thermo Fisher Scientific) and 25 µg/ml amphotericin B (Thermo Fisher Scientific) (Langan et al, 2015; Magerl et al, 2008) for 7–8 days.

Immunohistochemistry, immunofluorescence microscopy, and quantitative (immuno)histomorphometry

Cryosections (6 µm) were stained for Ki-67/TUNEL, LC3b, and gp100 immunofluorescence and MTCO1 and DCD reactivity (Supplementary Table S4). TUNEL immunofluorescence was performed using the ApopTag fluorescein *in situ* apoptosis detection kit (Merck), according to the manufacturer's instructions. Quantitative melanin histomorphometry was performed by Masson–Fontana, as previously described (Hardman et al, 2015).

Hair cycle assessment

Hair cycle staging and score were assessed histologically on the basis of morphology, Masson–Fontana, and Ki-67/TUNEL (immuno) histochemistry, as previously described (Klopper et al, 2010; Langan et al, 2015). Hair cycle score was calculated using an arbitrary score (anagen = 100, early catagen = 200, and mid-catagen = 300).

RNA extraction and RT-qPCR

For microbial RT-qPCR, total RNA was extracted from 2–3 full-length HFs. A total of 200 µl TRIzol (Thermo Fisher Scientific) were added to the HFs in a bead-beating extraction tube (Precellys, Bertin Technologies), and extraction was carried out with the Precellys Evolution Homogenizer (Bertin Instruments) with 5 × (20 seconds at 8000 r.p.m. and 30 seconds rest) at 4 °C, followed by 10,000g centrifugation for 5 minutes, 100 µl chloroform, and centrifugation at 10,000g for 5 minutes. The resulting aqueous phase was processed using the PicoPure kit (Applied Biosystems), according to the manufacturer's instructions. For RNA sequencing and butyrate treatment–induced AMP expression evaluation, total RNA was isolated from 3 HFs using the PicoPure RNA isolation kit (Applied Biosystems).

Bacterial RT-qPCR after *SEPI* infection was assessed by SYBR Green assay (Bio-Rad Laboratories), with *16S* ribosomal RNA gene (V1–V2), *C. acnes*–, and *S. epidermidis*–specific primers (Supplementary Table S3). *DCD*, *CAMP*, and *S100A7* expressions after butyrate were evaluated using Taqman assay and probes (Supplementary Table S3). Details are provided in Supplementary Materials and Methods.

RNA sequencing and bioinformatic analysis

Total RNA was sequenced using a NovaSeq 6000, 2 × 100 bp (30 M clusters per sample). Library was prepared with SMART-Seq Stranded Kit (Takara). Read demultiplexing was performed with Illumina bcl2fastq (2.20). Adapters were trimmed with Skewer (version 0.2.2) (Jiang et al, 2014), and reads were aligned to the GRCh38.105 using STAR (version 2.7.10a) (Dobin et al, 2013). Data were deposited in a public database and can be found under accession number GSE225849. Quality was analyzed with FastQC (version 0.11.9) (Andrews, 2010). Normalized counts were calculated with DESeq2 (version 1.30.1) (Love et al, 2014). Fold-change comparison between groups was done on the basis of normalized read counts ratio. Fold change was considered relevant if it was ≥2 (upregulation) or ≤0.5 (downregulation). An additional cutoff of counts per million mapped reads ≥0.5 was chosen for the transcript of interest (for upregulation) or for the reference (for downregulation). The DAVID online tool was used for Gene Ontology, Kyoto Encyclopedia of Genes and Genomes pathway, and functional annotations (Sherman et al, 2022).

Statistical analysis of immunofluorescence microscopy and RT-qPCR

Statistical analyses were performed using GraphPad Prism 9 (GraphPad Software). Given the common microbiome intra-individual variability and that each HF represents an individual miniorgan, each HF was statistically observed as a single entity (Jahns et al, 2015; Schneider et al, 2009). Data were assessed for normality with D'Agostino and Pearson omnibus normality test. Normally distributed datasets were compared with an unpaired *t*-test or 1-way ANOVA. The remaining datasets were compared with the nonparametric unpaired Mann-Whitney or Kruskal–Wallis tests. Data are expressed as mean ± SEM. *P* < .05 was considered significant. Further details are provided in Supplementary Materials and Methods.

DATA AVAILABILITY STATEMENT

Datasets related to this article can be found at <https://www.ncbi.nlm.nih.gov/Traces/study?acc=PRJNA937066>, <https://www.ncbi.nlm.nih.gov/Traces/study?acc=PRJNA937065>, and <https://www.ncbi.nlm.nih.gov/geo/query/acc.cgi?acc=GSE225849> hosted at the Sequence Read Archive and Gene Expression Omnibus databases, under accession numbers PRJNA937065, PRJNA937066, and GSE225849.

ORCID

Marta B. Lousada: <http://orcid.org/0000-0003-3142-663X>
Janin Edelkamp: <http://orcid.org/0000-0002-2050-3890>
Tim Lachnit: <http://orcid.org/0000-0002-2880-5930>
Markus Fehrholtz: <http://orcid.org/0000-0003-2183-2415>
Irena Pastar: <http://orcid.org/0000-0003-0197-6198>
Francisco Jimenez: <http://orcid.org/0000-0003-1676-3056>
Hanieh Erdmann: <http://orcid.org/0000-0002-2054-6428>
Thomas C. G. Bosch: <http://orcid.org/0000-0002-9488-5545>
Ralf Paus: <http://orcid.org/0000-0002-3492-9358>

CONFLICT OF INTEREST

JE and MF are employees of Monasterium Laboratory GmbH, for which FJ acts as a consultant. MLB and RP were employed by Monasterium Laboratory

during the execution of this study, and the latter is employed by CUTANEON. The remaining authors state no conflict of interest.

ACKNOWLEDGMENTS

The authors would like to thank Luís Melo from the Universidade do Minho for generously providing the *SEPI* phage used in this study and Dragana Ajdic and Michael Hoptroff for very helpful critical comments. This study was supported by a PhD fellowship to MBL, cosponsored by Giuliani S.p.a. (Milano, Italy) and Monasterium Laboratory (Münster, Germany), and an associated basic research grant from the latter. Research in the laboratory of TCGB is supported in part by grants from the Deutsche Forschungsgemeinschaft, the CRC 1182 “Origin and Function of Metaorganisms” (to TCGB and TL), and the CRC 1461 “Neurotronics: Bio-Inspired Information Pathways” (to TCGB). TCGB appreciates support from the Canadian Institute for Advanced Research. RP is supported by a Frost Endowed Scholarship from the Department of Dermatology, University of Miami.

AUTHOR CONTRIBUTIONS

Conceptualization: RP, TCGB, TL, JE, MBL; Data Curation: JE, TL, IP, MBL; Formal Analysis: MF; Investigation: MBL; Methodology: JE, MBL; Resources: FJ, HE; Supervision: JE, TL, TCGB, RP; Writing - Original Draft Preparation: MBL, JE, RP; Writing - Review and Editing: MBL, JE, TL, MF, IP, FJ, HE, TCGB, RP

SUPPLEMENTARY MATERIAL

Supplementary material is linked to the online version of the paper at www.jidonline.org, and at <https://doi.org/10.1016/j.jid.2023.11.006>.

REFERENCES

- Abreu CM, Cerqueira MT, Pirraco RP, Gasperini L, Reis RL, Marques AP. Rescuing key native traits in cultured dermal papilla cells for human hair regeneration. *J Adv Res* 2020;30:103–12.
- Alexeyev OA, Lundskog B, Ganceviciene R, Palmer RH, McDowell A, Patrick S, et al. Pattern of tissue invasion by *Propionibacterium acnes* in acne vulgaris. *J Dermatol Sci* 2012;67:63–6.
- Andl T, Zhou L, Zhang Y. The dermal papilla dilemma and potential breakthroughs in bioengineering hair follicles. *Cell Tissue Res* 2023;391:221–33.
- Andrews S. FastQC: a quality control tool for high throughput sequence data. <http://www.bioinformatics.babraham.ac.uk/projects/fastqc>; 2010. (accessed September 10, 2023).
- Arimoto K, Takahashi H, Hishiki T, Konishi H, Fujita T, Shimotohno K. Negative regulation of the RIG-I signaling by the ubiquitin ligase RNF125. *Proc Natl Acad Sci USA* 2007;104:7500–5.
- Bertolini M, McElwee K, Gilhar A, Bulfone-Paus S, Paus R. Hair follicle immune privilege and its collapse in alopecia areata. *Exp Dermatol* 2020;29:703–25.
- Bertolini M, Zilio F, Rossi A, Kleditzsch P, Emelianov VE, Gilhar A, et al. Abnormal interactions between perifollicular mast cells and CD8+ T-cells may contribute to the pathogenesis of alopecia areata. *PLoS One* 2014;9:e94260.
- Bispo Lousada MB, Edelkamp J, Lachnit T, Erdmann H, Paus R. Can antibiotic-induced changes in the composition of the hair follicle microbiome regulate human hair growth? *Exp Dermatol* 2021;30:1440–1.
- Bodó E, Kromminga A, Funk W, Lausch M, Duske U, Jelkmann W, et al. Human hair follicles are an extrarenal source and a nonhematopoietic target of erythropoietin. *FASEB J* 2007;21:3346–54.
- Bolger AM, Lohse M, Usadel B. Trimmomatic: a flexible trimmer for Illumina sequence data. *Bioinformatics* 2014;30:2114–20.
- Bouslimani A, Porto C, Rath CM, Wang M, Guo Y, Gonzalez A, et al. Molecular cartography of the human skin surface in 3D. *Proc Natl Acad Sci USA* 2015;112:E2120–9.
- Byrd AL, Belkaid Y, Segre JA. The human skin microbiome. *Nat Rev Microbiol* 2018;16:143–55.
- Cannons JL, Villarino AV, Kapnick SM, Preite S, Shih HY, Gomez-Rodriguez J, et al. PI3K coordinates transcriptional, chromatin, and metabolic changes to promote effector CD8+ T cells at the expense of central memory. *Cell Rep* 2021;37:109804.
- Castillo R, Subudhi I, Naik S. Fanning the flames: IRAK2 signaling in differentiated epithelium potentiates skin inflammation. *J Invest Dermatol* 2021;141:2325–7.

- Chai M, Jiang M, Vergnes L, Fu X, de Barros SC, Doan NB, et al. Stimulation of hair growth by small molecules that activate autophagy. *Cell Rep* 2019;27:3413–21.e3.
- Chéret J, Bertolini M, Ponce L, Lehmann J, Tsai T, Alam M, et al. Olfactory receptor OR2AT4 regulates human hair growth. *Nat Commun* 2018;9:3624.
- Chopra D, Arens RA, Amornpaiboj W, Lowes MA, Tomic-Canic M, Strbo N, et al. Innate immunity and microbial dysbiosis in hidradenitis suppurativa – vicious cycle of chronic inflammation. *Front Immunol* 2022;13:960488.
- Christoph T, Müller-Röver S, Audring H, Tobin DJ, Hermes B, Cotsarelis G, et al. The human hair follicle immune system: cellular composition and immune privilege. *Br J Dermatol* 2000;142:862–73.
- Claesen J, Spagnolo JB, Ramos SF, Kurita KL, Byrd AL, Aksenov AA, et al. A *Cutibacterium acnes* antibiotic modulates human skin microbiota composition in hair follicles. *Sci Transl Med* 2020;12:eaay5445.
- Clarke EL, Taylor LJ, Zhao C, Connell A, Lee JJ, Fett B, et al. Sunbeam: an extensible pipeline for analyzing metagenomic sequencing experiments. *Microbiome* 2019;7:46.
- Constantinou A, Kanti V, Polak-Witka K, Blume-Peytavi U, Spyrou GM, Vogt A. The potential relevance of the microbiome to hair physiology and regeneration: the emerging role of metagenomics. *Biomedicines* 2021a;9:236.
- Constantinou A, Polak-Witka K, Tomazou M, Oulas A, Kanti V, Schwarzer R, et al. Dysbiosis and enhanced beta-defensin production in hair follicles of patients with lichen planopilaris and frontal fibrosing alopecia. *Biomedicines* 2021b;9:266.
- Conwill A, Kuan AC, Damerla R, Poret AJ, Baker JS, Tripp AD, et al. Anatomy promotes neutral coexistence of strains in the human skin microbiome. *Cell Host Microbe* 2022;30:171–82.e7.
- Dobin A, Davis CA, Schlesinger F, Drenkow J, Zaleski C, Jha S, et al. STAR: ultrafast universal RNA-seq aligner. *Bioinformatics* 2013;29:15–21.
- Dubus M, Varin J, Papa S, Chevrier J, Quilès F, Francius G, et al. Bone marrow mesenchymal stem cells offer an immune-privileged niche to *Cutibacterium acnes* in case of implant-associated osteomyelitis. *Acta Biomater* 2022;137:305–15.
- Edelkamp J, Gherardini J, Bertolini M. Methods to study human hair follicle growth ex vivo: human microdissected hair follicle and human full thickness skin organ culture. *Methods Mol Biol* 2020;2154:105–19.
- Edelkamp J, Lousada MB, Pinto D, Chéret J, Calabrese FM, Jiménez F, et al. Management of the human hair follicle microbiome by a synthetic odorant. *J Dermatol Sci* 2023;112(2):99–108.
- El-Mahdy TS, Mongaret C, Varin-Simon J, Lamret F, Vernet-Garnier V, Rammal H, et al. Interaction of implant infection-related commensal bacteria with mesenchymal stem cells: a comparison between *Cutibacterium acnes* and *Staphylococcus aureus*. *FEMS Microbiol Lett* 2021;368:fnab014.
- Emelianov VU, Bechara FG, Gläser R, Langan EA, Taungjaruwina WM, Schröder JM, et al. Immunohistological pointers to a possible role for excessive cathelicidin (LL-37) expression by apocrine sweat glands in the pathogenesis of hidradenitis suppurativa/acne inversa. *Br J Dermatol* 2012;166:1023–34.
- Fan Y, Pedersen O. Gut microbiota in human metabolic health and disease. *Nat Rev Microbiol* 2021;19:55–71.
- Figlak K, Williams G, Bertolini M, Paus R, Philpott MP. Human hair follicles operate an internal Cori cycle and modulate their growth via glycogen phosphorylase. *Sci Rep* 2021;11:20761.
- Flowers L, Grice EA. The skin microbiota: balancing risk and reward. *Cell Host Microbe* 2020;28:190–200.
- Fournière M, Latire T, Souak D, Feuilloley MGJ, Bedoux G. *Staphylococcus epidermidis* and *Cutibacterium acnes*: two Major Sentinels of Skin microbiota and the Influence of Cosmetics. *Microorganisms* 2020;8:E1752.
- Garza LA, Liu Y, Yang Z, Alagesan B, Lawson JA, Norberg SM, et al. Prostaglandin D2 inhibits hair growth and is elevated in bald scalp of men with androgenetic alopecia. *Sci Transl Med* 2012;4:126ra34.
- Geyfman M, Plikus MV, Treffeisen E, Andersen B, Paus R. Resting no more: redefining telogen, the maintenance stage of the hair growth cycle. *Biol Rev Camb Philos Soc* 2015;90:1179–96.
- Grice EA, Segre JA. The skin microbiome [published correction appears in *Nat Rev Microbiol* 2011;9:626]. *Nat Rev Microbiol* 2011;9:244–53.
- Grogan MD, Bartow-McKenney C, Flowers L, Knight SAB, Ueberoi A, Grice EA. Research techniques made simple: profiling the skin microbiota. *J Invest Dermatol* 2019;139:747–52.e1.
- Hall JB, Cong Z, Imamura-Kawasawa Y, Kidd BA, Dudley JT, Thiboutot DM, et al. Isolation and identification of the follicular microbiome: implications for acne research. *J Invest Dermatol* 2018;138:2033–40.
- Hardman JA, Muneeb F, Pople J, Bhogal R, Shahmalak A, Paus R. Human perifollicular macrophages undergo apoptosis, express Wnt ligands, and switch their polarization during catagen. *J Invest Dermatol* 2019;139:2543–6.e9.
- Hardman JA, Tobin DJ, Haslam IS, Farjo N, Farjo B, Al-Nuaimi Y, et al. The peripheral clock regulates human pigmentation. *J Invest Dermatol* 2015;135:1053–64.
- Harris-Tryon TA, Grice EA. Microbiota and maintenance of skin barrier function. *Science* 2022;376:940–5.
- Häselbarth L, Ouwens DM, Teichweyde N, Hoerath K, Merches K, Esser C. The small chain fatty acid butyrate antagonizes the TCR-stimulation-induced metabolic shift in murine epidermal gamma Delta T cells. *EXCLI J* 2020;19:334–50.
- Ho BS-Y, Ho EXP, Chu CW, Ramasamy S, Bigliardi-Qi M, de Sessions PF, et al. Microbiome in the hair follicle of androgenetic alopecia patients. *PLoS One* 2019;14:e0216330.
- Ito T, Fukamizu H, Ito N, Seo N, Yagi H, Takigawa M, et al. Roxithromycin antagonizes catagen induction in murine and human hair follicles: implication of topical Roxithromycin as hair restoration reagent. *Arch Dermatol Res* 2009;301:347–55.
- Jahns AC, Alexeyev OA. Three dimensional distribution of *Propionibacterium acnes* biofilms in human skin. *Exp Dermatol* 2014;23:687–9.
- Jahns AC, Lundskog B, Berg J, Jonsson R, McDowell A, Patrick S, et al. Microbiology of folliculitis: a histological study of 39 cases. *APMIS* 2014;122:25–32.
- Jahns AC, Lundskog B, Nosek D, Killasli H, Emtestam L, Alexeyev OA. Microbiology of folliculitis decalvans: a histological study of 37 patients. *J Eur Acad Dermatol Venereol* 2015;29:1025–6.
- James AG, Abraham KH, Cox DS, Moore AE, Pople JE. Metabolic analysis of the cutaneous fungi *Malassezia globosa* and *M. restricta* for insights on scalp condition and dandruff. *Int J Cosmet Sci* 2013;35:169–75.
- Jensen PJ, Yang T, Yu DW, Baker MS, Risse B, Sun TT, et al. Serpins in the human hair follicle. *J Invest Dermatol* 2000;114:917–22.
- Jiang H, Lei R, Ding SW, Zhu S. Skewer: a fast and accurate adapter trimmer for next-generation sequencing paired-end reads. *BMC Bioinformatics* 2014;15:182.
- Jo H, Kim SY, Kang BH, Baek C, Kwon JE, Jeang JW, et al. *Staphylococcus epidermidis* Cicaria, a novel strain derived from the human microbiome, and its efficacy as a treatment for hair loss. *Molecules* 2022;27:5136.
- Kawano M, Komi-Kuramochi A, Asada M, Suzuki M, Oki J, Jiang J, et al. Comprehensive analysis of FGF and FGFR expression in skin: FGF18 is highly expressed in hair follicles and capable of inducing anagen from telogen stage hair follicles. *J Invest Dermatol* 2005;124:877–85.
- Kim CH. Control of lymphocyte functions by gut microbiota-derived short-chain fatty acids. *Cell Mol Immunol* 2021;18:1161–71.
- Kim HJ, Oh HN, Park T, Kim H, Lee HG, An S, et al. Aged related human skin microbiome and mycobiome in Korean women. *Sci Rep* 2022;12:2351.
- Kloepper JE, Sugawara K, Al-Nuaimi Y, Gáspár E, van Beek N, Paus R. Methods in hair research: how to objectively distinguish between anagen and catagen in human hair follicle organ culture. *Exp Dermatol* 2010;19:305–12.
- Kruglikov IL, Zhang Z, Scherer PE. Skin aging: dermal adipocytes metabolically reprogram dermal fibroblasts. *Bioessays* 2022;44:e2100207.
- Kuninaka Y, Ishida Y, Ishigami A, Nosaka M, Matsuki J, Yasuda H, et al. Macrophage polarity and wound age determination. *Sci Rep* 2022;12:20327.
- Langan EA, Philpott MP, Kloepper JE, Paus R. Human hair follicle organ culture: theory, application and perspectives. *Exp Dermatol* 2015;24:903–11.
- Larabi A, Barnich N, Nguyen HTT. New insights into the interplay between autophagy, gut microbiota and inflammatory responses in IBD. *Autophagy* 2020;16:38–51.

- Lemasters JJ, Ramshesh VK, Lovelace GL, Lim J, Wright GD, Harland D, et al. Compartmentation of mitochondrial and oxidative metabolism in growing hair follicles: a ring of fire. *J Invest Dermatol* 2017;137:1434–44.
- Li KN, Jain P, He CH, Eun FC, Kang S, Tumber T. Skin vasculature and hair follicle cross-talking associated with stem cell activation and tissue homeostasis. *Elife* 2019;8:e45977.
- Li Y, Zheng W, Lu Y, Zheng Y, Pan L, Wu X, et al. BNIP3L/NIX-mediated mitophagy: molecular mechanisms and implications for human disease. *Cell Death Dis* 2021;13:14.
- Liu Y, Elworth RAL, Jochum MD, Aagaard KM, Treangen TJ. De novo identification of microbial contaminants in low microbial biomass microbiomes with QIIME2. *Nat Commun* 2022;13:6799.
- Lousada MB, Edelkamp J, Lachnit T, Fehrholtz M, Jimenez F, Paus R. Laser capture microdissection as a method for investigating the human hair follicle microbiome reveals region-specific differences in the bacteriome profile. *BMC Res Notes* 2023;16:29.
- Lousada MB, Lachnit T, Edelkamp J, Rouillé T, Ajdic D, Uchida Y, et al. Exploring the human hair follicle microbiome. *Br J Dermatol* 2021;184:802–15.
- Love MI, Huber W, Anders S. Moderated estimation of fold change and dispersion for RNA-seq data with DESeq2. *Genome Biol* 2014;15:550.
- Lu J, Salzberg SL. Removing contaminants from databases of draft genomes. *PLoS Comput Biol* 2018;14:e1006277.
- Lu YJ, Sasaki T, Kuwahara-Arai K, Uehara Y, Hiramatsu K. Development of a new application for comprehensive viability analysis based on microbiome analysis by next-generation sequencing: insights into staphylococcal carriage in human nasal cavities. *Appl Environ Microbiol* 2018;84:e00517–8.
- Magerl M, Lammell V, Siebenhaar F, Zuberbier T, Metz M, Maurer M. Non-pathogenic commensal *Escherichia coli* bacteria can inhibit degranulation of mast cells. *Exp Dermatol* 2008;17:427–35.
- Markandey M, Bajaj A, Ilott NE, Kedia S, Travis S, Powrie F, et al. Gut microbiota: sculptors of the intestinal stem cell niche in health and inflammatory bowel disease. *Gut Microbes* 2021;13:1990827.
- Martin M. Cutadapt removes adapter sequences from high-throughput sequencing reads. *EMBnet.journal* 2011;17:10–2.
- Melo LDR, França A, Brandão A, Sillankorva S, Cerca N, Azeredo J. Assessment of Sep1virus interaction with stationary cultures by transcriptional and flow cytometry studies. *FEMS Microbiol Ecol* 2018;94.
- Melo LDR, Pinto G, Oliveira F, Vilas-Boas D, Almeida C, Sillankorva S, et al. The protective effect of *Staphylococcus epidermidis* biofilm matrix against phage predation. *Viruses* 2020;12:1076.
- Melo LDR, Sillankorva S, Ackermann HW, Kropinski AM, Azeredo J, Cerca N. Isolation and characterization of a new *Staphylococcus epidermidis* broad-spectrum bacteriophage. *J Gen Virol* 2014;95:506–15.
- Miao Q, Hill MC, Chen F, Mo Q, Ku AT, Ramos C, et al. SOX11 and SOX4 drive the reactivation of an embryonic gene program during murine wound repair. *Nat Commun* 2019;10:4042.
- Ng KJ, Lim J, Tan YN, Quek D, Lim Z, Pantelireis N, et al. Sox2 in the dermal papilla regulates hair follicle pigmentation. *Cell Rep* 2022;40:111100.
- Nicu C, O'Sullivan JDB, Ramos R, Timperi L, Lai T, Farjo N, et al. Dermal adipose tissue secretes HGF to promote human hair growth and pigmentation. *J Invest Dermatol* 2021;141:1633–45.e13.
- O'Neill AM, Gallo RL. Host-microbiome interactions and recent progress into understanding the biology of acne vulgaris. *Microbiome* 2018;6:177.
- O'Sullivan JDB, Nicu C, Picard M, Chéret J, Bedogni B, Tobin DJ, et al. The biology of human hair greying. *Biol Rev Camb Philos Soc* 2021;96:107–28.
- Park M, Cho YJ, Lee YW, Jung WH. Understanding the mechanism of action of the anti-dandruff agent zinc Pyrithione against *Malassezia restricta*. *Sci Rep* 2018;8:12086.
- Parodi C, Hardman JA, Allavena G, Marotta R, Catelani T, Bertolini M, et al. Autophagy is essential for maintaining the growth of a human (mini-)organ: evidence from scalp hair follicle organ culture. *PLoS Biol* 2018;16:e2002864.
- Paus R, Cotsarelis G. The biology of hair follicles. *N Engl J Med* 1999;341:491–7.
- Paus R, Foitzik K. In search of the “hair cycle clock”: a guided tour. *Differentiation* 2004;72:489–511.
- Pilkington SM, Ogden S, Eaton LH, Dearman RJ, Kimber I, Griffiths CEM. Lower levels of interleukin-1 β gene expression are associated with impaired Langerhans' cell migration in aged human skin. *Immunology* 2018;153:60–70.
- Pinto D, Sorbellini E, Marzani B, Rucco M, Giuliani G, Rinaldi F. Scalp bacterial shift in alopecia areata. *PLoS One* 2019;14:e0215206.
- Poblet E, Jimenez F, Escario-Travesedo E, Hardman JA, Hernández-Hernández I, Agudo-Mena JL, et al. Eccrine sweat glands associate with the human hair follicle within a defined compartment of dermal white adipose tissue. *Br J Dermatol* 2018;178:1163–72.
- Polak-Witka K, Constantinou A, Schwarzer R, Helmuth J, Wiessner A, Hadam S, et al. Identification of anti-microbial peptides and traces of microbial DNA in infrainfundibular compartments of human scalp terminal hair follicles. *Eur J Dermatol* 2021;31:22–31.
- Polak-Witka K, Rudnicka L, Blume-Peytavi U, Vogt A. The role of the microbiome in scalp hair follicle biology and disease. *Exp Dermatol* 2020;29:286–94.
- Polkoff KM, Gupta NK, Green AJ, Murphy Y, Chung J, Gleason KL, et al. LGR5 is a conserved marker of hair follicle stem cells in multiple species and is present early and throughout follicle morphogenesis. *Sci Rep* 2022;12:9104.
- Probst AJ, Auerbach AK, Moissl-Eichinger C. Archaea on Human Skin. *PLoS One* 2013;8:e65388.
- Purba TS, Berriche L, Paus R. Compartmentalised metabolic programmes in human anagen hair follicles: new targets to modulate epithelial stem cell behaviour, keratinocyte proliferation and hair follicle immune status? *Exp Dermatol* 2021;30:645–51.
- Ratajczak W, Rył A, Mizerski A, Walczakiewicz K, Sipak O, Laszczyńska M. Immunomodulatory potential of gut microbiome-derived short-chain fatty acids (SCFAs). *Acta Biochim Pol* 2019;66:1–12.
- Reithmayer K, Meyer KC, Kleditzsch P, Tiede S, Uppalapati SK, Gläser R, et al. Human hair follicle epithelium has an antimicrobial defence system that includes the inducible antimicrobial peptide psoriasin (S100A7) and RNase 7. *Br J Dermatol* 2009;161:78–89.
- Rinaldi F, Pinto D, Borsani E, Castrezzati S, Amedei A, Rezzani R. The First Evidence of Bacterial Foci in the Hair Part and Dermal Papilla of Scalp Hair Follicles: A Pilot Comparative Study in Alopecia Areata. *Int J Mol Sci* 2022;23(19):11956.
- Ring HC, Sigsgaard V, Thorsen J, Fuursted K, Fabricius S, Saunte DM, et al. The microbiome of tunnels in hidradenitis suppurativa patients. *J Eur Acad Dermatol Venereol* 2019;33:1775–80.
- Rittié L, Stoll SW, Kang S, Voorhees JJ, Fisher GJ. Hedgehog signaling maintains hair follicle stem cell phenotype in young and aged human skin. *Aging Cell* 2009;8:738–51.
- Salter SJ, Cox MJ, Turek EM, Calus ST, Cookson WO, Moffatt MF, et al. Reagent and laboratory contamination can critically impact sequence-based microbiome analyses. *BMC Biol* 2014;12:87.
- Schneider MR, Schmidt-Ullrich R, Paus R. The hair follicle as a dynamic miniorgan. *Curr Biol* 2009;19:R132–42.
- Schwarz A, Bruhs A, Schwarz T. The short-chain fatty acid sodium butyrate functions as a regulator of the skin immune system. *J Invest Dermatol* 2017;137:855–64.
- Sevilla A, Chéret J, Lee W, Paus R. Concentration-dependent stimulation of melanin production as well as melanocyte and keratinocyte proliferation by melatonin in human eyelid epidermis. *Exp Dermatol* 2023;32:684–93.
- Sherman BT, Hao M, Qiu J, Jiao X, Baseler MW, Lane HC, et al. DAVID: a web server for functional enrichment analysis and functional annotation of gene lists (2021 update). *Nucleic Acids Res* 2022;50:W216–21.
- Sibaud V. Dermatologic reactions to immune checkpoint inhibitors : skin toxicities and immunotherapy. *Am J Clin Dermatol* 2018;19:345–61.
- Silva GGZ, Green KT, Dutilh BE, Edwards RA. SUPER-FOCUS: a tool for agile functional analysis of shotgun metagenomic data. *Bioinformatics* 2016;32:354–61.
- Silveira GDP, Ishimura ME, Teixeira D, Galindo LT, Sardinha AA, Porcionatto M, et al. Improvement of mesenchymal stem cell

- immunomodulatory properties by heat-killed *Propionibacterium acnes* via TLR2. *Front Mol Neurosci* 2019;11:489.
- Slominski A, Wortsman J, Luger T, Paus R, Solomon S. Corticotropin releasing hormone and proopiomelanocortin involvement in the cutaneous response to stress. *Physiol Rev* 2000;80:979–1020.
- Suzuki T, Chéret J, Scala FD, Akhundlu A, Gherardini J, Demetrius DL, et al. mTORC1 activity negatively regulates human hair follicle growth and pigmentation. *EMBO Rep* 2023;24:e56574.
- Tang Y, Luo B, Deng Z, Wang B, Liu F, Li J, et al. Mitochondrial aerobic respiration is activated during hair follicle stem cell differentiation, and its dysfunction retards hair regeneration. *PeerJ* 2016;4:e1821.
- Tiede S, Hundt JE, Paus R. UDP-GlcNAc-1-Phosphotransferase is a clinically important regulator of human and mouse hair pigmentation. *J Invest Dermatol* 2021;141:2957–65.e5.
- Traisaeng S, Herr DR, Kao HJ, Chuang TH, Huang CM. A derivative of butyric acid, the fermentation metabolite of *Staphylococcus epidermidis*, inhibits the growth of a *Staphylococcus aureus* Strain isolated from atopic dermatitis patients. *Toxins* 2019;11:311.
- Trompette A, Pernet J, Perdijk O, Alqahtani RAA, Domingo JS, Camacho-Muñoz D, et al. Gut-derived short-chain fatty acids modulate skin barrier integrity by promoting keratinocyte metabolism and differentiation. *Mucosal Immunol* 2022;15:908–26.
- Tsuru A, Hamazaki Y, Tomida S, Ali MS, Komura T, Nishikawa Y, et al. Nonpathogenic *Cutibacterium acnes* confers host resistance against *Staphylococcus aureus*. *Microbiol Spectr* 2021;9:e0056221.
- Umbach AK, Stegelmeier AA, Neufeld JD. Archaea are rare and uncommon members of the mammalian skin microbiome. *mSystems* 2021;6:e00642–21.
- Vidali S, Chéret J, Giesen M, Haeger S, Alam M, Watson REB, et al. Thyroid hormones enhance mitochondrial function in human epidermis. *J Invest Dermatol* 2016;136:2003–12.
- Vidali S, Knuever J, Lerchner J, Giesen M, Bíró T, Klinger M, et al. Hypothalamic–pituitary–thyroid axis hormones stimulate mitochondrial function and biogenesis in human hair follicles. *J Invest Dermatol* 2014;134:33–42.
- Voigt AY, Emiola A, Johnson JS, Fleming ES, Nguyen H, Zhou W, et al. Skin microbiome variation with cancer progression in human cutaneous squamous cell carcinoma. *J Invest Dermatol* 2022;142:2773–82.e16.
- Wang Y, Yan Y, Thompson KN, Bae S, Accorsi EK, Zhang Y, et al. Whole microbial community viability is not quantitatively reflected by propidium monoazide sequencing approach. *Microbiome* 2021;9:17.
- Williams R, Pawlus AD, Thornton MJ. Getting under the skin of hair aging: the impact of the hair follicle environment. *Exp Dermatol* 2020;29:588–97.
- Wood DE, Lu J, Langmead B. Improved metagenomic analysis with Kraken 2. *Genome Biol* 2019;20:257.
- Wu L, Zeng T, Deligios M, Milanese L, Langille MGI, Zinellu A, et al. Age-related variation of bacterial and fungal communities in different body habitats across the young, elderly, and centenarians in Sardinia. *mSphere* 2020;5:e00558–19.
- Wu Z, Meyer-Hoffert U, Reithmayer K, Paus R, Hansmann B, He Y, et al. Highly complex peptide aggregates of the S100 fused-type protein hornerin are present in human skin. *J Invest Dermatol* 2009;129:1446–58.
- Yao Y, Frew JW, Thomsen SF, Ring HC. Antimicrobial peptides in hidradenitis suppurativa: a systematic review. *Br J Dermatol* 2022;186:236–44.
- Yoon SY, Detmar M. Sostdc1 secreted from cutaneous lymphatic vessels acts as a paracrine factor for hair follicle growth. *Curr Issues Mol Biol* 2022;44:2167–74.
- Zari J, Abdolmajid F, Masood M, Vahid M, Yalda N. Evaluation of the relationship between androgenetic alopecia and demodex infestation. *Indian J Dermatol* 2008;53:64–7.
- Zhu N, Lin E, Zhang H, Liu Y, Cao G, Fu C, et al. LncRNA H19 Overexpression Activates Wnt Signaling to Maintain the Hair Follicle Regeneration Potential of Dermal Papilla Cells. *Front Genet* 2020;11:694 H19.

SUPPLEMENTARY TEXT S1

Gammaretrovirus murine leukemia virus dominated the virome in all HF compartments, with the exception of the suprabulbar region, where *Gemycircularvirus Pteropus*–associated *Gemycircularvirus* 10 was more predominant (Supplementary Figure S3a). These were followed by colonization with *Propionibacterium* phages in all compartments and *Pseudomonas* phages also within the DP. Interestingly, these translated into a higher representation of the top most abundant species in the epithelial tissues, which were dominated by *Gammaretrovirus* murine leukemia virus, *G Pteropus*–associated *Gemycircularvirus* 10, and *Faecalibacterium* phages, a profile similar to the virome composition of older donors (Supplementary Figure S3b and c).

In contrast, the top 10 archaeal species were more abundant in the bulb region, whereas the DP registered the lowest diversity (Supplementary Figure S3d). Most interestingly, although *Natronomonas* sp YPL13 and *Mathanobrevibacter smithii* were more abundant in the epithelium, the mesenchyme registered a higher abundance of *Halomicrobium* sp LC1Hm and *Halopenitus persicus* (Supplementary Figure S3e). Variations in these communities were also found with age, where *Halalkalicoccus jeotgali* and *Saccharolobus solfataricus* were more abundant in younger donors, whereas *M smithii* and *Natronomonas* sp YPL13 were more abundant in older donors (Supplementary Figure S3f).

SUPPLEMENTARY TEXT S2

Propidium monoazide (PMA) is a photoreactive dye that covalently binds free DNA and DNA from nonintact membrane cells, given that it does not penetrate viable membrane cells, to allow selective investigation and profiling of membrane-intact microorganisms (Joo et al., 2019; Lee et al., 2022). Hence, PMA treatment chemically reduces the contribution of free DNA and allows the enriched evaluation of viable microbes (Joo et al., 2019; Lee et al., 2022). Although this technique provides a better overview of the viable commensals, it has been shown to not quantitatively represent the entirety of the viable microbial communities in complex samples, mostly overrepresenting these communities and underrepresenting low-abundance microorganisms (Wang et al, 2021). Furthermore, result variations according to PMA concentration, light intensity, incubation time, and the analyzed tissue have also been reported (Mancabelli et al, 2021; Wang et al, 2021).

SUPPLEMENTARY TEXT S3

The skin and HF microbiota species *Staphylococcus epidermidis* and *Cutibacterium acnes* are regarded as beneficial bacteria given their protective role against pathogens such as *S. aureus* (Fournière et al, 2020). Indeed, both these species were shown to inhibit pathogenic *S. aureus* growth, biofilm formation, and virulence, through the production of bacteriocins, metalloproteinases, phenol-soluble modulins, and short-chain fatty acids (Fournière et al, 2020). Furthermore, some *S. epidermidis* strains have shown inhibitory activity against certain *C. acnes* isolates, whereas *C. acnes* inhibited *S. epidermidis* biofilm formation (Christensen et al, 2016; Claudel et al, 2019).

Interestingly, in contrast with these previously reported interactions, the *SEP1* bacteriophage therapy–induced decrease in *S. epidermidis* abundance resulted in a decrease in *C. acnes* and an increase in *S. aureus* abundance. Despite this, this community regulation pattern was previously observed in HF cultures, where the increase in *Staphylococcus* correlated with the decrease in *Cutibacterium* (Bispo Lousada et al, 2021). Hence, the decrease in *S. epidermidis* likely resulted in the observed *S. aureus* increase and thereby *C. acnes* decrease. Therefore, these data further suggest that although *S. aureus* in healthy scalp HFs does not represent the top 10 abundant species, its abundance is increased in culture or by the depletion of *S. epidermidis*, a phenomenon often observed in dysbiosis, for example, in hidradenitis suppurativa (Chopra et al, 2022; Świerczewska et al, 2022; Wark and Cains, 2021).

SUPPLEMENTARY TEXT S4

Several bacterial metabolites, such as short-chain fatty acids, have been shown to modulate human biology, particularly in the gut microbiome (Portincasa et al, 2022). Among these, butyrate is produced by various of the identified HF colonizers, including *Faecalibacterium*, *Pseudomonas*, and *S. epidermidis* (Kircher et al, 2022; Thompson et al, 2020; Traisaeng et al, 2019). The latter metabolize butyrate in the presence of glycerol, which in the HF can be obtained by sebaceous gland triglyceride hydrolysis (Choi et al, 2005; Fluhr et al, 2003; Negari et al, 2021). Interestingly, this metabolite was found to promote epithelial cell metabolism and barrier function in the human gut (Sanford et al., 2019; Trompette et al., 2022). Furthermore, a role of butyrate in lipid and glucose metabolism, mitochondrial function, autophagy, prevention of ROS and nitric oxide production, and inflammation has been reported (Hu et al., 2020; Zhang et al., 2021, 2022). This is important in the current HF biology context because autophagic flux in the human hair matrix and intrafollicular energy metabolism are important determinants of anagen duration (Figlak et al, 2021; Parodi et al, 2018). Hence, the role of butyrate on HF growth, metabolism, autophagy, and antimicrobial peptide expression (dermcidin) was assessed.

SUPPLEMENTARY TEXT S5

Limitations of our study that deserve to be considered when interpreting our data include the low number of samples that could be investigated, the usual pitfalls of low biomass studies (Kennedy et al, 2023), and the preliminary nature of our functional pilot analyses, all of which require confirmation/validation in follow-up studies to permit definitive conclusions. Yet, in contrast to the findings in some previous human microbiome studies, the likelihood of contamination during the clinical procedure (Kennedy et al, 2023) is very low because the scalp skin surface was rigorously disinfected before surgery, followed by sterile HF microdissection free of extrafollicular tissue. Despite its limitations, the combination of metagenomic shotgun sequencing of defined, anatomical HF compartments assessed by laser-capture microdissection (including functional microbiome profiling); FISH confirmation of the intrafollicular localization of 2 selected microbiota; viability testing; and functional microbiome manipulation by HF infection with an *S. epidermis*–specific bacteriophage presented in this study

provides, to our knowledge, the most comprehensive characterization of the human scalp HF microbiota available to date and generates intriguing leads that inform and guide follow-up work.

SUPPLEMENTARY TEXT S6

Interesting variations in the abundance profile and respective functional potential according to donor age were also observed. Namely, there was an increase in the abundance of *M. restricta* and *C. acnes* in relation to the HF microbiota profile in older donors (Figure 1d), together with a decrease in the functional profile. Nevertheless, individually, the abundance of these microbes decreased with age (Figure 1e and f). Although given the limited number of individuals evaluated in this study ($n = 5$), the lack of analysis of these data after PMA treatment, since only 2 donors were assessed, and the high interindividual variations observed in these data should be corroborated; these are in line with skin microbiome age difference evaluations (Kim et al, 2022; Luna, 2020). Hence, these variations could be reflective of age-related environmental differences and possibly the epidemiology of HF diseases. Although acne vulgaris mainly affects younger individuals, androgenetic alopecia primarily affects patients aged >50 years, with both featuring *C. acnes* dysbiosis (Layton et al, 2021; Ho et al, 2022, 2019). It is thought that these derive from age-related changes in HF biology, particularly the hormonal alterations in adolescence, which could drive the observed dysbiosis and promote disease pathobiology (Ho et al, 2022; Park et al, 2022).

SUPPLEMENTARY MATERIALS AND METHODS

RT-qPCR

Bacterial RT-qPCR after *SEP1* infection was assessed by SYBR Green assay (Bio-Rad Laboratories) in triplicates, with *16S* ribosomal RNA gene (V1–V2), *C. acnes*–, and *S. epidermidis*–specific primers (Supplementary Table S2). Each qPCR reaction mixture consisted of SYBR Green qPCR Mix (Bio-Rad Laboratories), and 400 nM of each primer was reverse transcribed using the Tetro cDNA synthesis kit (Bioline International), according to the manufacturer's instructions. The amplification program consisted of an initial denaturation step at 95 °C for 10 minutes, followed by 40 cycles of denaturation at 95 °C for 30 seconds, and annealing at 60 °C for 1 minute, followed by a melt curve stage at 95 °C for 15 seconds, 60 °C for 1 minute, and 95 °C for 1 second. *DCD*, *CAMP*, and *S100A7* expressions after butyrate were evaluated in triplicates using Taqman probes (Supplementary Table S2) and protocol (Thermo Fisher Scientific). Reactions were assessed using Quantstudio3 Real-Time PCR system with the associated software (Applied Biosystems).

qRT-PCR statistical methodology

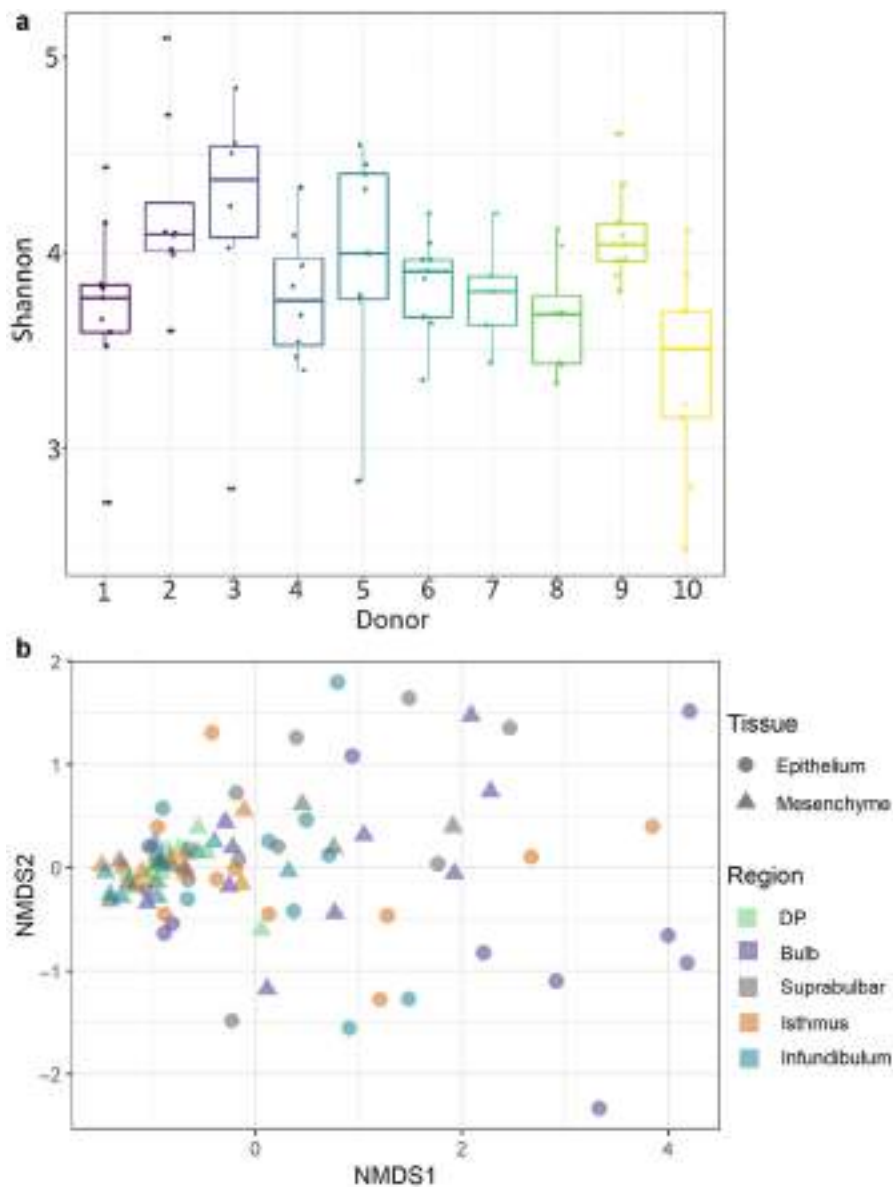
Since following phage infection, total bacterial load, as evaluated by *16S* ribosomal RNA gene expression, varied between the experimental groups, bacterial RT-qPCR was normalized to the human housekeeping gene *GAPDH* and quantified after this normalization. For RT-qPCR analysis, undetermined values were assumed to correspond to the

highest amount of amplification cycles used (40) to allow for evaluation of expression changes.

SUPPLEMENTARY REFERENCES

- Bispo Lousada MB, Edelkamp J, Lachnit T, Erdmann H, Paus R. Can antibiotic-induced changes in the composition of the hair follicle microbiome regulate human hair growth? *Exp Dermatol* 2021;30:1440–1.
- Brakstad OG, Aasbakk K, Maeland JA. Detection of *Staphylococcus aureus* by polymerase chain reaction amplification of the nuc gene. *J Clin Microbiol* 1992;30:1654–60.
- Campiche R, Le Riche A, Edelkamp J, Botello AF, Martin E, Gempeler M, et al. An extract of *Leontopodium alpinum* inhibits catagen development ex vivo and increases hair density in vivo. *Int J Cosmet Sci* 2022;44:363–76.
- Cao L, Tian T, Huang Y, Tao S, Zhu X, Yang M, et al. Neural progenitor cell-derived nanovesicles promote hair follicle growth via miR-100. *J Nanobiotechnology* 2021;19:20.
- Chéret J, Bertolini M, Ponce L, Lehmann J, Tsai T, Alam M, et al. Olfactory receptor OR2AT4 regulates human hair growth. *Nat Commun* 2018;9:3624.
- Choi EH, Man M-Q, Wang F, Zhang X, Brown BE, Feingold KR, et al. Is endogenous glycerol a determinant of stratum corneum hydration in humans? *J Gen Intern Med* 2005;20:288–93.
- Chopra D, Arens RA, Amornpairoj W, Lowes MA, Tomic-Canic M, Strbo N, et al. Innate immunity and microbial dysbiosis in hidradenitis suppurativa – vicious cycle of chronic inflammation. *Front Immunol* 2022;13:960488.
- Christensen GJM, Scholz CFP, Enghild J, Rohde H, Kilian M, Thürmer A, et al. Antagonism between *Staphylococcus epidermidis* and *Propionibacterium acnes* and its genomic basis. *BMC Genomics* 2016;17:152.
- Claudel J-P, Auffret N, Leccia M-T, Poli F, Corvec S, Dréno B. *Staphylococcus epidermidis*: a potential new player in the physiopathology of acne? *Dermatology* 2019;235:287–94.
- Figlak K, Williams G, Bertolini M, Paus R, Philpott MP. Human hair follicles operate an internal Cori cycle and modulate their growth via glycogen phosphorylase. *Sci Rep* 2021;11:20761.
- Flores R, Shi J, Gail MH, Gajer P, Ravel J, Goedert JJ. Assessment of the human fecal microbiota: II. Reproducibility and associations of 16S rRNA pyrosequences. *Eur J Clin Invest* 2012;42:855–63.
- Fuhr JW, Mao-Qiang M, Brown BE, Wertz PW, Crumrine D, Sundberg JP, et al. Glycerol regulates stratum corneum hydration in sebaceous gland deficient (asebia) mice. *J Invest Dermatol* 2003;120:728–37.
- Fournière M, Latire T, Souak D, Feuilloley MGJ, Bedoux G. *Staphylococcus epidermidis* and *Cutibacterium acnes*: two Major Sentinels of Skin microbiota and the Influence of Cosmetics. *Microorganisms* 2020;8:E1752.
- Hardman JA, Tobin DJ, Haslam IS, Farjo N, Farjo B, Al-Nuaimi Y, et al. The peripheral clock regulates human pigmentation. *J Invest Dermatol* 2015;135:1053–64.
- Ho BS-Y, Ho EXP, Chu CW, Ramasamy S, Bigliardi-Qi M, de Sessions PF, et al. Microbiome in the hair follicle of androgenetic alopecia patients. *PLoS One* 2019;14:e0216330.
- Ho CH, Sood T, Zito PM. Androgenetic Alopecia. *StatPearls*. Treasure Island (FL). StatPearls Publishing; 2022. <http://www.ncbi.nlm.nih.gov/books/NBK430924/>. (accessed November 8, 2023).
- Hu S, Kuwabara R, de Haan BJ, Smink AM, de Vos P. Acetate and butyrate improve β -cell metabolism and mitochondrial respiration under oxidative stress. *Int J Mol Sci* 2020;21:1542.
- Joo S, Park P, Park S. Applicability of propidium monoazide (PMA) for discrimination between living and dead phytoplankton cells. *PLoS One* 2019;14:e0218924.
- Kennedy KM, de Goffau MC, Perez-Muñoz ME, Arrieta M-C, Bäckhed F, Bork P, et al. Questioning the fetal microbiome illustrates pitfalls of low-biomass microbial studies. *Nature* 2023;613:639–49.
- Kim HJ, Oh HN, Park T, Kim H, Lee HG, An S, et al. Aged related human skin microbiome and mycobiome in Korean women. *Sci Rep* 2022;12:2351.

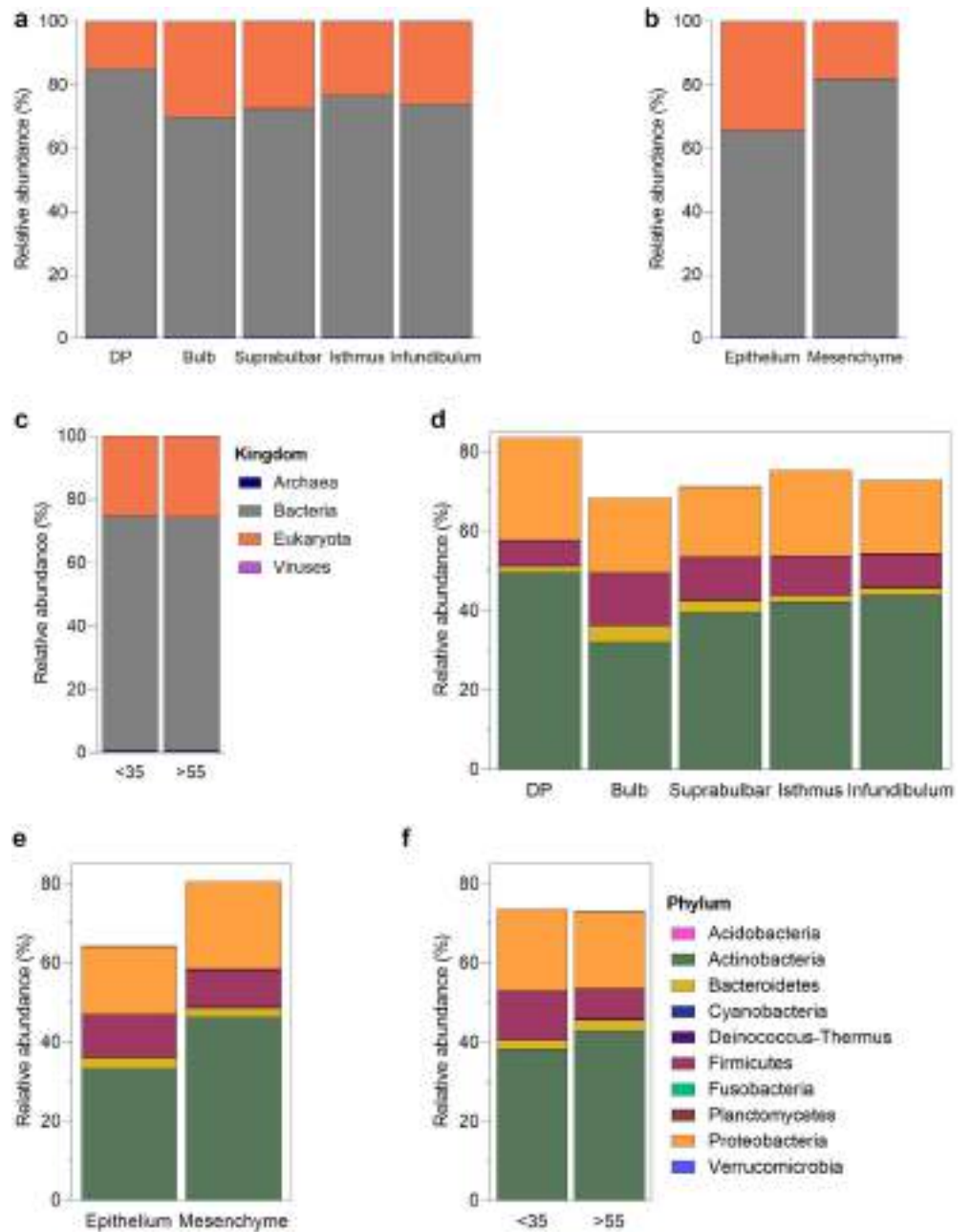
- Kircher B, Woltemate S, Gutzki F, Schlüter D, Geffers R, Bähre H, et al. Predicting butyrate- and propionate-forming bacteria of gut microbiota from sequencing data. *Gut Microbes* 2022;14:2149019.
- Kloepper JE, Sugawara K, Al-Nuaimi Y, Gáspár E, van Beek N, Paus R. Methods in hair research: how to objectively distinguish between anagen and catagen in human hair follicle organ culture. *Exp Dermatol* 2010;19:305–12.
- Layton AM, Thiboutot D, Tan J. Reviewing the global burden of acne: how could we improve care to reduce the burden? *Br J Dermatol* 2021;184:219–25.
- Lee AS, Lamanna OK, Ishida K, Hill E, Nguyen A, Hsieh MH. A novel propidium monoazide-based pcr assay can measure viable uropathogenic *E. coli* in vitro and in vivo. *Front Cell Infect. Microbiol* 2022;12:794323.
- Luna PC. Skin microbiome as years go by. *Am J Clin Dermatol* 2020;21(Suppl 1):12–7.
- Mancabelli L, Milani C, Anzalone R, Alessandri G, Lugli GA, Tarracchini C, et al. Free DNA and Metagenomics Analyses: Evaluation of Free DNA Inactivation Protocols for Shotgun Metagenomics Analysis of Human Biological Matrices. *Front Microbiol* 2021;12:749373.
- McDowell A, Valanne S, Ramage G, Tunney MM, Glenn JV, McLorinan GC, et al. Propionibacterium acnes types I and II represent phylogenetically distinct groups. *J Clin Microbiol* 2005;43:326–34.
- Negari IP, Keshari S, Huang C-M. Probiotic Activity of Staphylococcus epidermidis Induces Collagen Type I Production through FFA2/p-ERK Signaling. *Int J Mol Sci* 2021;22:1414.
- Park J, Schwardt NH, Jo J-H, Zhang Z, Pillai V, Phang S, et al. Shifts in the Skin Bacterial and Fungal Communities of Healthy Children Transitioning through Puberty. *J Invest Dermatol* 2022;142:212–9.
- Parodi C, Hardman JA, Allavena G, Marotta R, Catelani T, Bertolini M, et al. Autophagy is essential for maintaining the growth of a human (mini-)organ: evidence from scalp hair follicle organ culture. *PLoS Biol* 2018;16:e2002864.
- Portincasa P, Bonfrate L, Vacca M, De Angelis M, Farella I, Lanza E, et al. Gut Microbiota and Short Chain Fatty Acids: Implications in Glucose Homeostasis. *Int J Mol Sci* 2022;23:1105.
- Sanford JA, O'Neill AM, Zouboulis CC, Gallo RL. Short-chain fatty acids from Cutibacterium acnes activate both a canonical and epigenetic inflammatory response in human sebocytes. *J Immunol* 2019;202:1767–76.
- Schindelin J, Arganda-Carreras I, Frise E, Kaynig V, Longair M, Pietzsch T, et al. Fiji: an open-source platform for biological-image analysis. *Nat Methods*. Nature Publishing Group 2012;9:676–82.
- Świerczewska Z, Lewandowski M, Surowiecka A, Barańska-Rybak W. Microbiome in hidradenitis suppurativa—what we know and where we are heading. *Int J Mol Sci* 2022;23:11280.
- Thompson MG, Incha MR, Pearson AN, Schmidt M, Sharpless WA, Eiben CB, et al. Fatty acid and alcohol metabolism in pseudomonas putida: functional analysis using random barcode transposon sequencing. *Appl Environ Microbiol* 2020;86:e01665–720.
- Traisaeng S, Herr DR, Kao HJ, Chuang TH, Huang CM. A derivative of butyric acid, the fermentation metabolite of Staphylococcus epidermidis, inhibits the growth of a Staphylococcus aureus Strain isolated from atopic dermatitis patients. *Toxins (Basel)* 2019;11:311.
- Trompette A, Pernot J, Perdijk O, Alqahtani RAA, Domingo JS, Camacho-Muñoz D, et al. Gut-derived short-chain fatty acids modulate skin barrier integrity by promoting keratinocyte metabolism and differentiation. *Mucosal Immunol* 2022;15:908–26.
- Vidali S, Kneuver J, Lerchner J, Giesen M, Bíró T, Klinger M, et al. Hypothalamic–pituitary–thyroid axis hormones stimulate mitochondrial function and biogenesis in human hair follicles. *J Invest Dermatol* 2014;134:33–42.
- Wang Y, Yan Y, Thompson KN, Bae S, Accorsi EK, Zhang Y, et al. Whole microbial community viability is not quantitatively reflected by propidium monoazide sequencing approach. *Microbiome* 2021;9:17.
- Wark KJL, Cains GD. The microbiome in hidradenitis suppurativa: a review. *Dermatol Ther*. Springer 2021;11:39.
- Zhang L, Liu C, Jiang Q, Yin Y. Butyrate in energy metabolism: there is still more to learn. *Trends Endocrinol Metab*. TEM 2021;32:159–69.
- Zhang Y, Xu S, Qian Y, He X, Mo C, Yang X, et al. Sodium butyrate attenuates rotenone-induced toxicity by activation of autophagy through epigenetically regulating PGC-1 α expression in PC12 cells. *Brain Res* 2022;1776:147749.

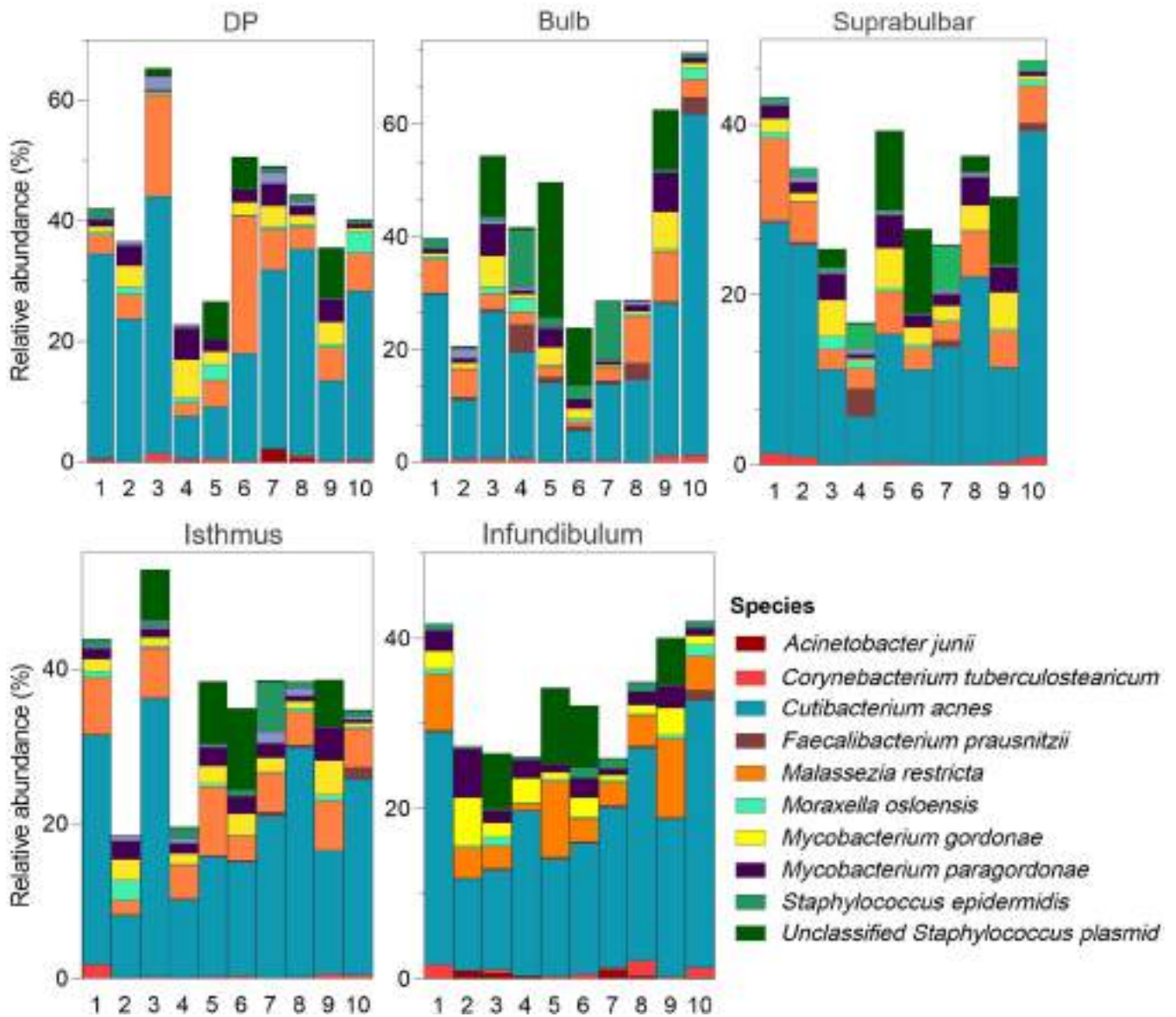


Supplementary Figure S1. Alpha-diversity based on the Shannon diversity index between donors and NMDS plot for beta-diversity patterns based on Bray–Curtis distances between HF regions and tissue lineages. Shotgun metagenomic sequencing of healthy unmanipulated HFs after LCM was performed, dividing the HFs into 5 anatomical regions (DP, bulb, suprabulbar, isthmus, and infundibulum) and 2 main tissue lineages (epithelium and mesenchyme). **(a)** Alpha-diversity comparison between the ten donors evaluated as measured by the Shannon-diversity index. **(b)** Beta-diversity comparison between the two HF tissue lineages (indicated by symbol shape) and between the five HF regions (indicated by symbol color), as measured by the Bray-Curtis distances. Scheirer–Ray–Hare nonparametric test was performed; $*P < .05$ (Shannon diversity index). Data are from $n = 10$ donors, corresponding to $n = 5$ HFs per donor. DP, dermal papilla; HF, hair follicle; LCM, laser-capture microdissection; NMDS, nonmetric multidimensional scaling.

Supplementary Figure S2. Shotgun metagenomic sequencing of healthy unmanipulated HFs after LCM.

Relative abundance of the identified HF microbiome (a–c) kingdoms and (d–f) the top 10 bacteria phyla, compared between each of the (a, d) 5 HF anatomically distinct regions, (b, e) 2 main tissue lineages, and (c, f) donor age groups. Data were pooled from n = 10 donors (for a and b and d and e) and n = 5 donors per group (for c and f), corresponding to n = 5 HFs per donor. DP, dermal papilla; HF, hair follicle; LCM, laser-capture microdissection.

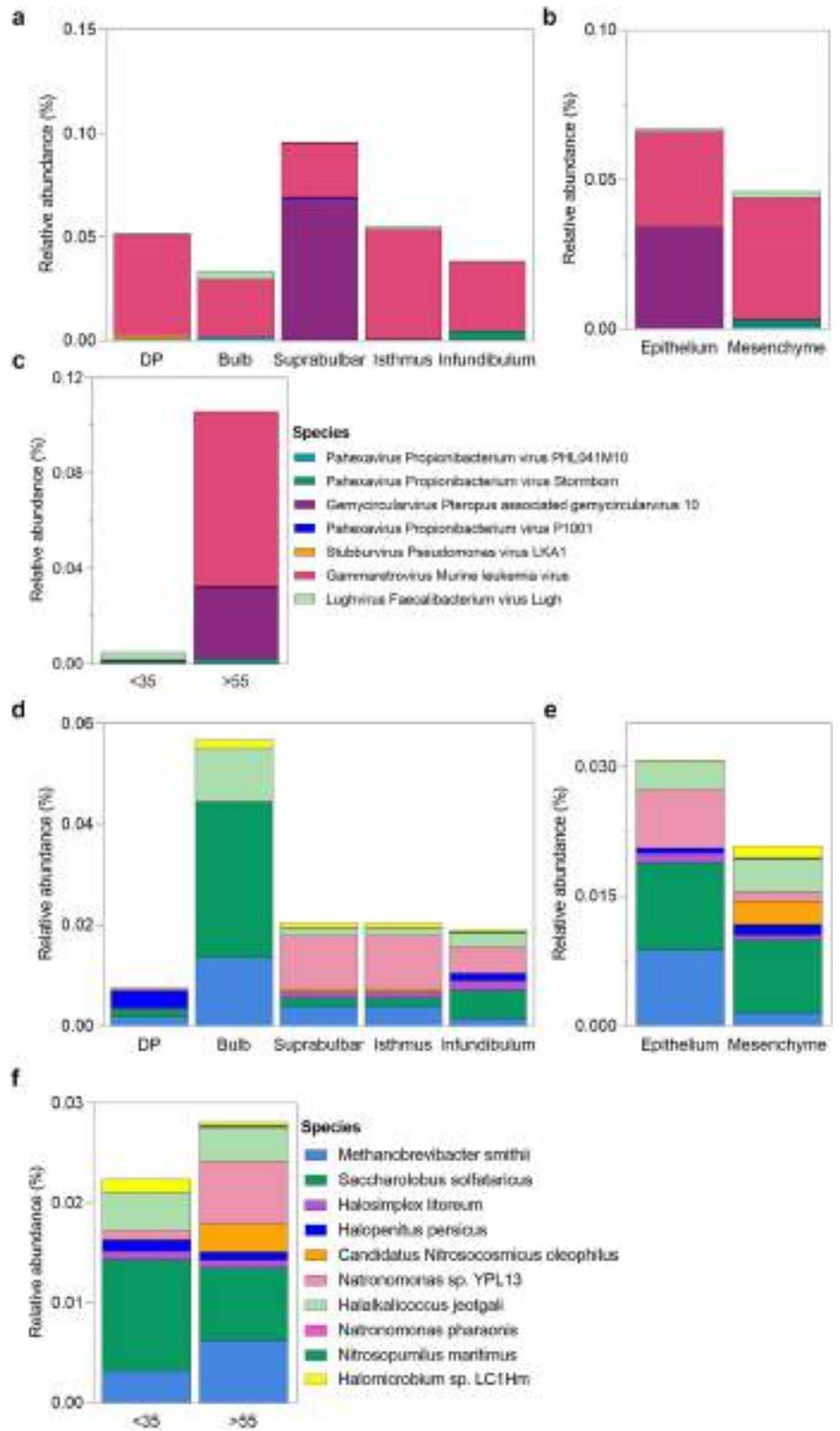


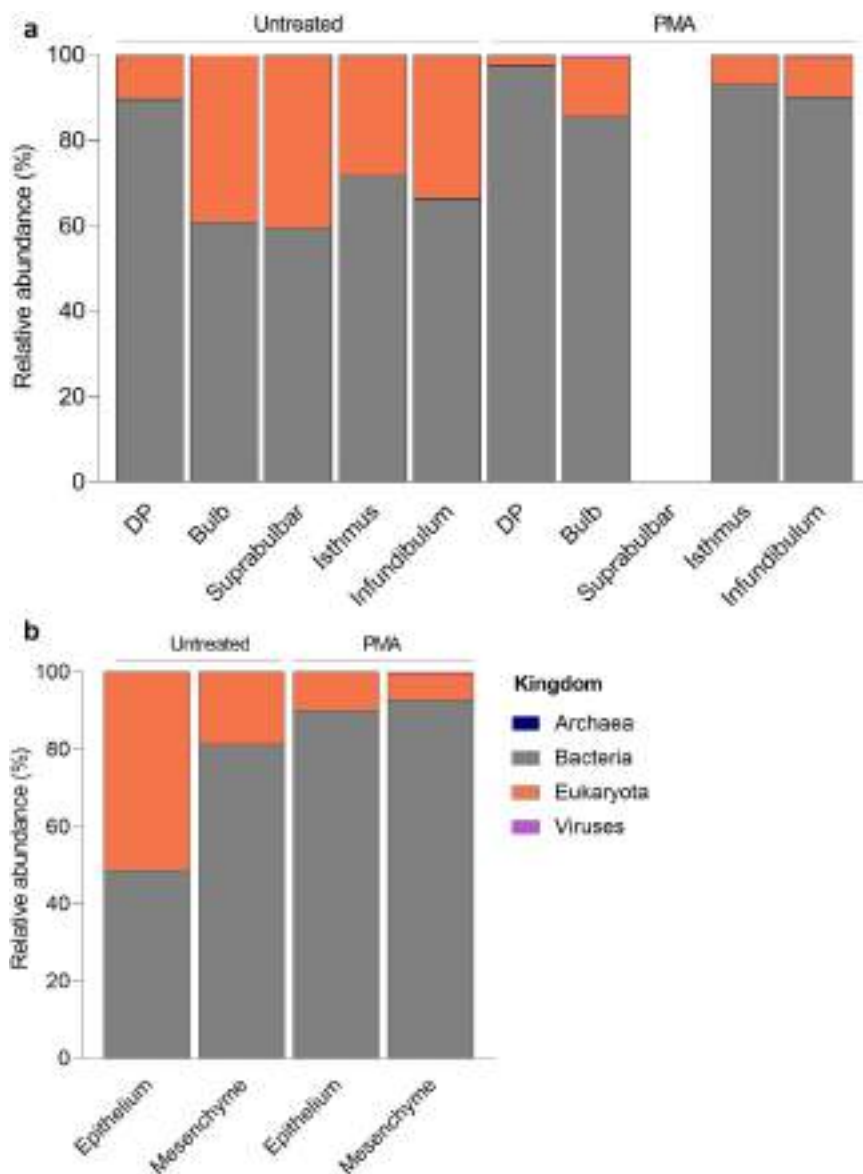


Supplementary Figure S3. Shotgun metagenomic sequencing of healthy unmanipulated HFs after LCM. Relative abundance of the top 10 main bacterial and fungal species found in each HF compartment (DP, bulb, suprabulbar, isthmus and infundibulum) per donor (each bar representing an individual male donor) is shown. Data were from n = 10 donors, corresponding to n = 5 HFs per donor. DP, dermal papilla; HF, hair follicle; LCM, laser-capture microdissection.

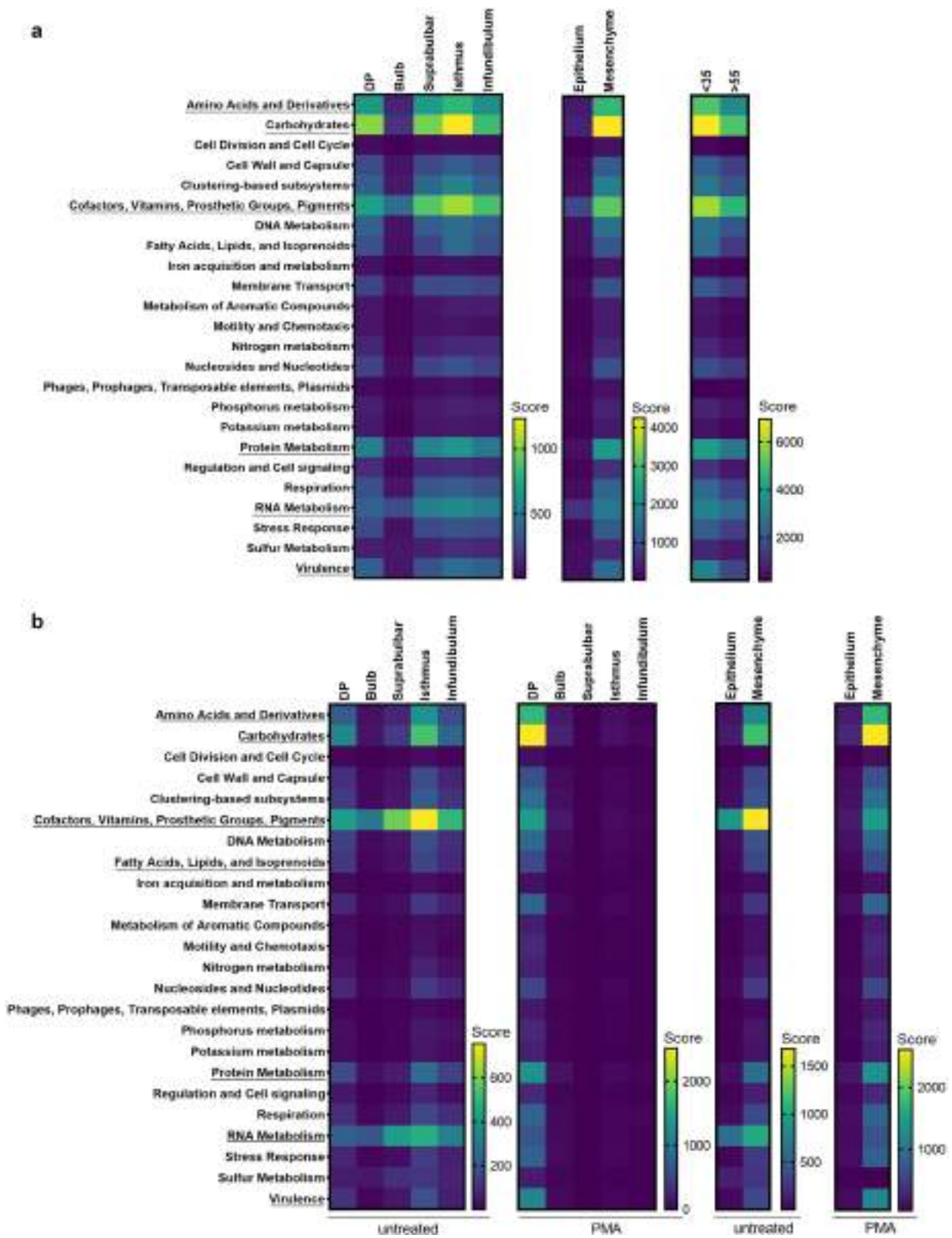
Supplementary Figure S4. Viral and archaeal HF microbiota composition varies according to region, tissue lineage, and donor age group.

Shotgun metagenomic sequencing of healthy unmanipulated HFs after LCM was performed. Relative abundance of the main viral species found in the HF compared between (a) each of the 5 HF anatomically distinct regions, (b) the 2 main HF tissue lineage tissue types, and (c) the donor age group is shown. Relative abundance of the top 10 main archaeal species found in the HF compared between (d) each of the 5 HF anatomically distinct regions, (e) the 2 main HF tissue lineage tissue types, and (f) donor age group is shown. Data were pooled from n = 10 donors (for a and b and d and e) and n = 5 donors each (for c and f), corresponding to n = 5 HFs per donor. DP, dermal papilla; HF, hair follicle; LCM, laser-capture microdissection.

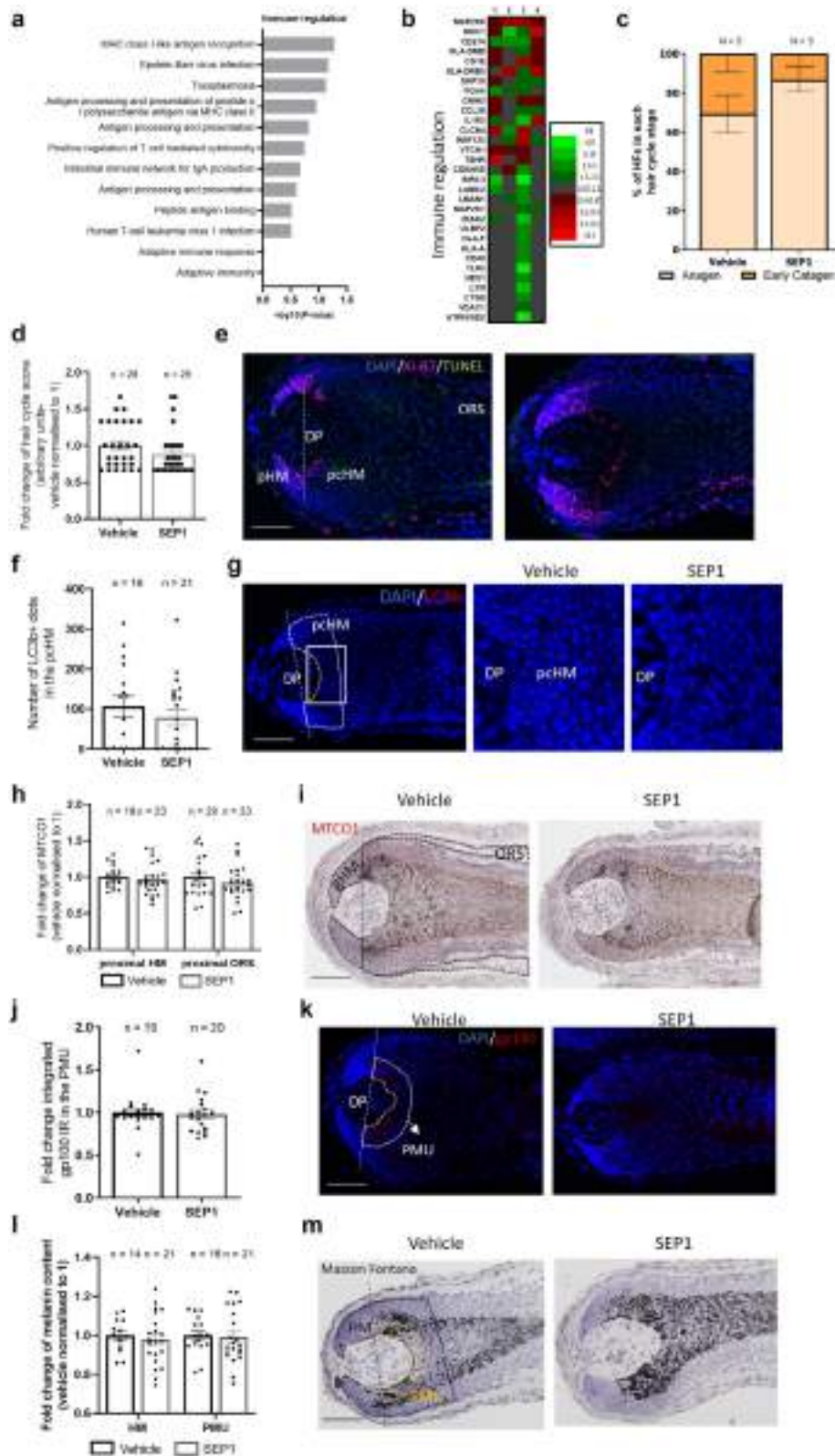




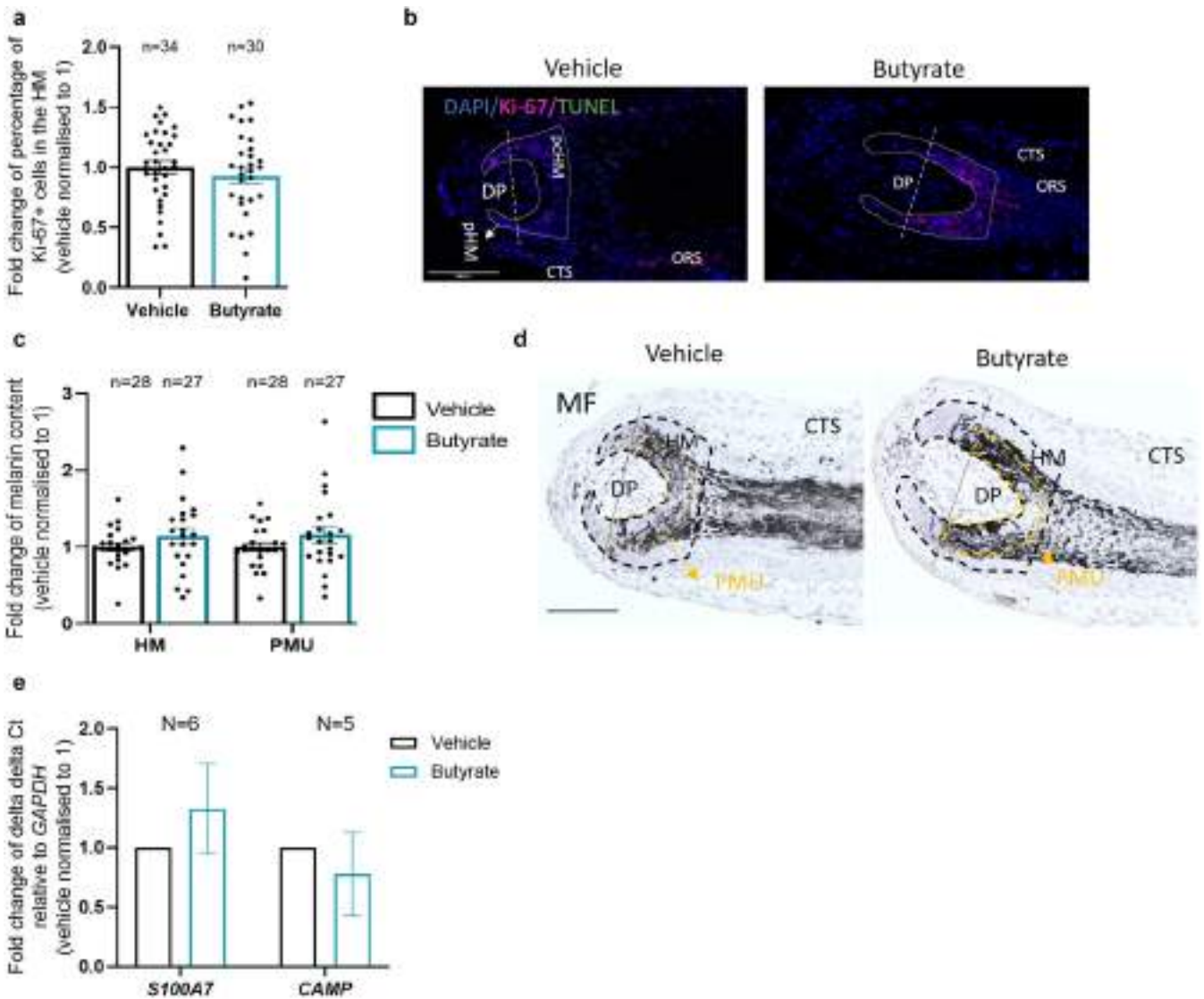
Supplementary Figure S5. PMA shotgun metagenomic sequencing of healthy unmanipulated HFs after LCM. Relative abundance of the HF microbiota kingdoms compared between (a) each of the 5 HF anatomically distinct regions and (b) the 2 main HF tissue lineages after PMA treatment is shown. Interestingly, PMA treatment depleted the HF bacteriota and mycobiota in the suprabulbar area, showing no reads in this HF compartment. Data were pooled from $n = 2$ donors, corresponding to $n = 5$ HFs per donor. DP, dermal papilla; HF, hair follicle; LCM, laser-capture microdissection; PMA, propidium monoazide.



Supplementary Figure S6. Predicted functional profile of the HF microbiota exhibits variations according to HF region, tissue lineage, and donor age group. High-quality reads from the generated shotgun metagenomic sequencing libraries were used to infer the functional profile of pathway enrichment on the basis of microbiota-derived genes. Normalized corresponding heat map comparison of the pathways with the most genetic representation among the HF microbiota between (a) untreated HF regions, tissue lineages, and donor age group and (b) PMA-treated HF regions and tissue lineages was performed. Underlined processes represent the pathways that varied the most between comparisons. Data were pooled from n = 10 (for a) and n = 2 (for b) donors, corresponding to n = 5 HFs per donor. DP, dermal papilla; HF, hair follicle; PMA, propidium monoazide.



Supplementary Figure S7. *SEPI* bacteriophage treatment and *S. epidermidis* abundance restriction alter HF biology. Healthy microdissected HF were cultured in the absence of antibiotics and the presence of SM buffer (vehicle) or *SEPI* bacteriophages and evaluated by RT-qPCR and RNA sequencing after 30 h of bacteriophage infection. (a) Significantly enriched immune regulation gene clusters found by RNA sequencing within the genes regulated only by *SEPI* treatment and respective *P*-adjusted values, as found by GO, KEGG pathway, and functional annotation analysis cluster with the DAVID online tool (Sherman et al, 2022), and (b) respective heat map RNA-sequencing comparison of *SEPI* treatment with vehicle control displaying the differentially regulated genes in the immune regulation cluster. Data are from $n = 4$ donors, corresponding to $n = 2$ HF per donor. (c) Percentage of catagen HF, as staged on the basis of MF histochemistry and Ki-67/TUNEL immunofluorescence. (d) Hair cycle score (in arbitrary units: 100 [anagen] and 200 [early catagen]). Pooled data are from $n = 5$ donors, corresponding to $n = 28$ –29 full-length HF. (e) Respective Ki-67/TUNEL representative images. (f) Number of L3Cb dots within the precortical hair



Supplementary Figure S8. Butyrate treatment does not affect intrafollicular Ki-67, melanin, *S100A7*, and *CAMP* expression. Healthy microdissected HFs were cultured for 7–8 days in the presence of antibiotics, with Williams complete medium only (vehicle) or 1 mM butyrate. **(a)** Fold change of the number of proliferative (Ki-67–positive) hair matrix keratinocytes after butyrate treatment, as evaluated in catagen and anagen HFs, and **(b)** respective representative images. **(c)** Fold change of melanin content in anagen VI HFs after treatment with butyrate within the HM and PMU assessed by MF histochemistry, and **(d)** respective representative images, with delineated analyzed areas. Bar = 100 μ m. Data from $n = 8$ donors, corresponding to $n = 27$ – 34 HFs, are represented as mean \pm SEM. D’Agostino and Pearson omnibus normality test, Gaussian distribution, unpaired t -test (for **c**), and Mann–Whitney test (for **a**) were performed, compared with the vehicle. **(e)** Psoriasin (*S100A7*) and LL-37 (*CAMP*) gene expression changes after 24 h of treatment with butyrate as measured by RT-qPCR. Results are expressed as mean \pm SEM from $n = 5$ – 6 donors, corresponding to $n = 3$ HFs per donor. h, hour; HF, hair follicle; HM, hair matrix; MF, Masson–Fontana; PMU, pigmentary unit.

matrix of anagen VI HFs and **(g)** respective representative images, with the area of evaluation marked in white. **(h)** MTCO1 immunohistochemistry in the pHM and ORS of anagen VI HFs and **(i)** respective representative images, with the areas of evaluation delineated. **(j)** Integrated gp100 immunofluorescence in the pigmentary unit of anagen VI HFs, and **(k)** respective representative images, with the area of evaluation delineated. **(l)** Fold change of melanin content in anagen VI HFs after treatment with butyrate within the HM and PMU assessed by MF histochemistry and **(m)** respective representative images, with the areas of evaluation delineated. Data from $n = 5$ donors, corresponding to $n = 16$ – 23 anagen VI HFs, are presented as mean \pm SEM. D’Agostino and Pearson omnibus normality test, no Gaussian distribution, Kruskal–Wallis test, and Mann–Whitney test, n.s., were performed; bars = 100 μ m. GO, Gene Ontology; h, hour; HF, hair follicle; HM, hair matrix; KEGG, Kyoto Encyclopedia of Genes and Genomes; MF, Masson–Fontana; n.s., not significant; ORS, outer root sheath; pHM, proximal hair matrix; PMU, pigmentary unit.

Supplementary Table S1. Donor Information

Experiment	Figures	Donor Demographics	Donor Material
Shotgun metagenomics and FISH	Figures 1 and 3 and Supplementary Figures S1–4 and S6a	10 males: 5 aged 22–34 + 5 aged 57–64 y	Occipital scalp HFs
Shotgun metagenomics—PMA treatment	Figure 2 and Supplementary Figures S5 and S6b	2 males: aged 59 and 64 y	Occipital scalp HFs
Bacteriophage therapy and RNA sequencing	Figure 4a–h and Supplementary Figure S7a and b	3 males: aged 27–40 y + 1 female: aged 54 y	Occipital and supraauricular scalp HFs
Bacteriophage therapy and protein expression	Figure 4i–k and Supplementary Figure S7c–m	5 males: aged 35–58 y	Occipital and temporal scalp HFs
Butyrate treatment	Figure 5 and Supplementary Figure S8	7 males: aged 29–66 y + 5 females: aged 20–66 y	Occipital and forehead HFs

Abbreviations: HF, hair follicle; PMA, propidium monoazide.

Supplementary Table S2. DNA Concentrations Measured by QuBit Assay before Metagenomic Shotgun Sequencing

Sample	DNA Concentration (ng/μl)	Sample	DNA Concentration (ng/μl)	Sample	DNA Concentration (ng/μl)
Donor 1 DP	0.102	Donor 5 DP	0.244	Donor 9 DP	Below threshold
Donor 1 bulb mesenchyme	0.364	Donor 5 bulb mesenchyme	0.544	Donor 9 bulb mesenchyme	0.188
Donor 1 bulb epidermis	1.7	Donor 5 bulb epidermis	2.1	Donor 9 bulb epidermis	Below threshold
Donor 1 suprabulbar mesenchyme	0.108	Donor 5 suprabulbar mesenchyme	0.248	Donor 9 suprabulbar mesenchyme	Below threshold
Donor 1 suprabulbar epidermis	0.56	Donor 5 suprabulbar epidermis	0.846	Donor 9 suprabulbar epidermis	0.242
Donor 1 isthmus mesenchyme	Below threshold	Donor 5 isthmus mesenchyme	0.132	Donor 9 isthmus mesenchyme	0.116
Donor 1 isthmus epidermis	0.262	Donor 5 isthmus epidermis	0.506	Donor 9 isthmus epidermis	Below threshold
Donor 1 infundibulum mesenchyme	Below threshold	Donor 5 infundibulum mesenchyme	Below threshold	Donor 9 infundibulum mesenchyme	Below threshold
Donor 1 infundibulum epidermis	0.346	Donor 5 infundibulum epidermis	0.256	Donor 9 infundibulum epidermis	0.142
Donor 1 negative control	Below threshold	Donor 5 negative control	Below threshold	Donor 9 negative control	Below threshold
Donor 2 DP	below threshold	Donor 6 DP	Below threshold	Donor 10 DP	Below threshold
Donor 2 bulb mesenchyme	0.214	Donor 6 bulb mesenchyme	0.286	Donor 10 bulb mesenchyme	0.306
donor 2 bulb epidermis	1.82	Donor 6 bulb epidermis	1.05	Donor 10 bulb epidermis	0.588
donor 2 Suprabulbar mesenchyme	0.104	Donor 6 suprabulbar mesenchyme	0.26	Donor 10 suprabulbar mesenchyme	Below threshold
Donor 2 suprabulbar epidermis	0.292	Donor 6 suprabulbar epidermis	0.802	Donor 10 suprabulbar epidermis	Below threshold
Donor 2 isthmus mesenchyme	0.118	Donor 6 isthmus mesenchyme	0.128	Donor 10 isthmus mesenchyme	Below threshold
Donor 2 isthmus epidermis	0.616	Donor 6 isthmus epidermis	0.254	Donor 10 isthmus epidermis	0.176
Donor 2 infundibulum mesenchyme	0.214	Donor 6 infundibulum mesenchyme	Below threshold	Donor 10 infundibulum mesenchyme	0.1
Donor 2 infundibulum epidermis	0.35	Donor 6 infundibulum epidermis	Below threshold	Donor 10 infundibulum epidermis	0.17
Donor 2 negative control	Below threshold	Donor 6 negative control	Below threshold	Donor 10 negative control	Below threshold
Donor 3 DP	Below threshold	Donor 7 DP	0.36		
Donor 3 bulb mesenchyme	0.208	donor 7 bulb mesenchyme	0.5		
Donor 3 bulb epidermis	Below threshold	Donor 7 bulb epidermis	2.28		
Donor 3 suprabulbar mesenchyme	Below threshold	Donor 7 suprabulbar mesenchyme	0.434		
Donor 3 suprabulbar epidermis	Below threshold	Donor 7 suprabulbar epidermis	1.01		
Donor 3 isthmus mesenchyme	Below threshold	Donor 7 isthmus mesenchyme	0.136		
Donor 3 isthmus epidermis	Below threshold	Donor 7 isthmus epidermis	0.234		
Donor 3 infundibulum mesenchyme	0.208	Donor 7 infundibulum mesenchyme	0.172		
Donor 3 infundibulum epidermis	Below threshold	donor 7 infundibulum epidermis	0.396		
Donor 3 negative control	Below threshold	Donor 7 negative control	Below threshold		
Donor 4 DP	Below threshold	Donor 8 DP	Below threshold		
Donor 4 bulb mesenchyme	0.56	Donor 8 bulb mesenchyme	0.288		
Donor 4 bulb epidermis	2.22	Donor 8 bulb epidermis	1.21		
Donor 4 suprabulbar mesenchyme	0.21	Donor 8 suprabulbar mesenchyme	0.104		
Donor 4 suprabulbar epidermis	0.75	Donor 8 suprabulbar epidermis	0.708		
Donor 4 isthmus mesenchyme	0.188	Donor 8 isthmus mesenchyme	0.152		
Donor 4 isthmus epidermis	1.23	Donor 8 isthmus epidermis	0.36		
Donor 4 infundibulum mesenchyme	Below threshold	Donor 8 infundibulum mesenchyme	0.15		
Donor 4 infundibulum epidermis	1.02	Donor 8 infundibulum epidermis	0.294		
Donor 4 negative control	0.214	Donor 8 negative control	Below threshold		

Abbreviation: DP, dermal papilla.

Supplementary Table S3. Nucleotide Sequences and Probes Used

Probe Name	Description	Sequence	Reference
16S	RNAscope Probe – EB-16S-rRNA-C2	—	ACDBio, catalog number 464461-C2
<i>C. acnes</i>	RNAscope Probe – <i>Propionibacterium acnes</i> -16S	—	ACDBio, catalog number 31393
<i>S. epidermidis</i>	RNAscope Probe – <i>S. epidermidis</i> -16S	—	ACDBio, catalog number 562431
DapB	RNAscope Negative Control Probe	—	ACDBio, catalog number, 310043
27F	qPCR universal bacterial 16S forward primer	5'-AGAGTTTGATCCTGGCTCAG-3'	Flores et al, 2012
338R	qPCR universal bacterial 16S reverse primer	5'-TGCTGCCTCCCGTAGGAGT-3'	Flores et al, 2012
<i>S. epidermidis F</i>	qPCR <i>S. epidermidis</i> -specific forward primer	5'-ATTGATGACGATGCGCCTTT-3'	This study
<i>S. epidermidis R</i>	qPCR <i>S. epidermidis</i> -specific reverse primer	5'-TGCTCTGCAAGAGATTGAC-3'	This study
PAR-1	qPCR <i>C. acnes</i> -specific forward primer	5'-AGCTCGGTGGGGTTCTCTCATC-3'	McDowell et al., 2005
PAR-2	qPCR <i>C. acnes</i> -specific reverse primer	5'-GCTTCCTCATACCACTGGTCATC-3'	McDowell et al., 2005
nucF	qPCR <i>S. aureus</i> -specific forward primer	5'-GCGATTGATGGTGATACGGTT-3'	Brakstad et al., 1992
nucR	qPCR <i>S. aureus</i> -specific reverse primer	5'-AGCCAAGCCTTGACGAACAAAGC-3'	Brakstad et al., 1992
DCD	Taqman dermcidin probe	—	Catalog number Hs01556562_g1 (Applied Biosystems)
CAMP	Taqman LL-37 probe	—	Catalog number Hs00189038_m1 (Applied Biosystems)
S100A7	Taqman psoriasin probe	—	Catalog number Hs00161488_m1 (Applied Biosystems)
GAPDH	Taqman GAPDH probe	—	Catalog number Hs99999905_m1 (Applied Biosystems)

Abbreviation: rRNA, ribosomal RNA.

Supplementary Table S4. Summary of the IF and IHC Staining Protocols Used

Target	Ki-67	LC3b	MTCO1	Gp100	DCD
Fixation	4% PFA	Acetone	Acetone	Acetone	4% PFA
Blocking	10% normal goat serum	10% normal goat serum	3% H ₂ O ₂	—	Avidin-biotin blocking kit (Vector Laboratories)
Primary antibody	1:800 Mouse-Anti human Ki-67 (Cell Signalling Technology) (Campiche et al, 2022; Cao et al, 2021)	1:400 rabbit anti-human LC3B D11 (Cell Signalling Technology) (Vidali et al, 2014)	1:800 rabbit anti-MTCO1 (Abcam) (Vidali et al, 2014)	1:200 Mouse anti-human NK1-beteb (Monosan) (Campiche et al, 2019)	1:500 Rabbit anti-human DCD (Atlas Antibodies)
Secondary antibody	Goat anti-mouse IgG –Rhodamine Red (Jackson ImmunoResearch)	Goat anti-rabbit IgG Rhodamine (Jackson ImmunoResearch)	Goat anti-rabbit –biotinylated (Jackson ImmunoResearch)	Goat anti-mouse Rhodamine (Jackson ImmunoResearch)	Goat anti-rabbit biotinylated (Jackson ImmunoResearch)
Amplification system/ chromogen	Rhodamine Red	Rhodamine Red	ABC-alkaline phosphatase kit (VectaStain) and AEC kit (Vector Laboratories)	Rhodamine Red	ABC-alkaline phosphatase kit (VectaStain) and Alkaline Phosphatase Fast Red tablets (Merck)
Washing buffer	PBS	PBS	TBS	PBS	TBS
Counterstain	DAPI	DAPI	Hematoxylin	DAPI	Hematoxylin
Negative controls	Omission of primary antibody, and negative immunoreactivity in tissue compartments/cells that typically do not express the antigen				
Internal positive control	Correspondence with previously published antigen expression patterns in human skin or HFs (Chéret et al, 2018; Parodi et al, 2018; Vidali et al, 2014)				
Analysis	Proximal hair matrix (Kloepper et al, 2010)	Precortical hair matrix of anagen VI HFs (Parodi et al, 2018)	Proximal hair matrix and ORS (Schindelin et al., 2012; Vidali et al, 2014)	Pigmentary unit of anagen VI HFs (Hardman et al, 2015)	Intrafollicular epithelium (Chéret et al, 2018)

Abbreviations: H₂O₂, hydrogen peroxide; HF, hair follicle; PFA, paraformaldehyde; ORS, outer root sheath.

Supplementary Table S5. BLAST Identification of the Unclassified *Staphylococcus* Plasmid Sequences

Description	Scientific Name	E-Value	Percentage of Identity (%)	Accession
<i>Clostridium Botulinum</i> strain Mfbjulcb6 chromosome, complete genome	<i>Clostridium botulinum</i>	2e-68	98.68	NZ_CP027778.1
<i>Bacillus amyloliquefaciens</i> strain CAS02 plasmid unnamed, complete sequence	<i>Bacillus amyloliquefaciens</i>	2e-68	98.68	CP071933.1
<i>Staphylococcus epidermidis</i> strain 48 plasmid pSE48-4, complete sequence	<i>Staphylococcus epidermidis</i>	2e-68	98.68	CP090928.1